

A Time-Varying Distributed Unit Hydrograph method considering soil moisture

Bin Yi^{1,2}, Lu Chen^{1,2*}, Hansong Zhang^{1,3}, Vijay P. Singh⁴, Ping Jiang⁵, Yizhuo Liu^{1,2},

Hexiang Guo^{1,2}, Hongya Qiu^{1,6}

¹ School of Civil and Hydraulic Engineering, Huazhong University of Science and Technology, Wuhan,

430074, China

² Hubei Key Laboratory of Digital Valley Science and Technology, Wuhan 430074, China

³ Power China Huadong Engineering Corporation Limited, Hangzhou 310014, China

⁴ Department of Biological & Agricultural Engineering, and Zachry Department of Civil & Environmental Engineering, Texas A&M University, College Station, Texas 77843-2117, USA; National Water and Energy Center, UAE University, Al Ain, UAE

⁵ Meizhou Hydrological Bureau, Guangdong Province, Meizhou 514000, China

⁶ China Three Gorges Corporation, Yichang 443133, China

Correspondence: Lu Chen (chen_lu@hust.edu.cn)

Abstract: The distributed unit hydrograph (DUH) method has been widely used for flow routing in a watershed, because it adequately characterizes the underlying surface characteristics and varying rainfall intensity. Fundamental to the calculation of DUH is flow velocity. However, the currently used velocity formula assumes a global equilibrium of the watershed and ignores the impact of time-varying soil moisture content on flow velocity, which thus leads to a larger flow velocity. The objective of

删除的内容: content

删除的内容: .

删除的内容: .

带格式的: 上标

带格式的: 上标

删除的内容: .

带格式的: 字体: 五号, 上标

25 this study was to identify a soil moisture content factor, which, based on the tension
 26 water storage capacity curve, was derived to investigate the response of DUH to soil
 27 moisture content in unsaturated areas. Thus, an improved distributed unit hydrograph,
 28 based on time-varying soil moisture content, was obtained. The proposed DUH
 29 considered the impact of both time-varying rainfall intensity and soil moisture content
 30 on flow velocity, assuming the watershed to be not in equilibrium but varying with soil
 31 moisture. The Qin River basin and Longhu River basin were selected as two case
 32 studies, and the synthetic unit hydrograph (SUH), time-varying distributed unit
 33 hydrograph (TDUH), and the current DUH methods were compared with the proposed
 34 method. Then, the influence of time-varying soil moisture content on flow velocity and
 35 flow routing was evaluated, and results showed that the proposed method performed the
 36 best among the four methods. The shape and duration of the unit hydrograph (UH) were
 37 mainly related to the soil moisture content at the initial stage of a rainstorm, and when
 38 the watershed was approximately saturated, the grid flow velocity was mainly
 39 dominated by excess rainfall. The proposed method can be used for the watersheds with
 40 sparse gauging stations and limited observed rainfall and runoff data.

41 **Keywords:** Time-varying distributed unit hydrograph, Runoff routing, Flow velocity,
 42 Soil moisture content, Excess rainfall

43 **1. Introduction**

44 Flow routing is an essential component of a hydrological model, whose accuracy

删除的内容: is was

删除的内容: developed

删除的内容: the

删除的内容: ,

删除的内容: .

删除的内容: A

删除的内容: a

删除的内容:

删除的内容: T

删除的内容: the

删除的内容: . R

删除的内容: can

删除的内容: be

删除的内容: . When

删除的内容: is

删除的内容: is

删除的内容: In addition,

删除的内容: T

删除的内容: t

删除的内容: -

删除的内容: important

删除的内容: in

67 directly affects runoff prediction and forecasting. Different types of flow routing
 68 techniques are available, such as hydraulic and hydrologic methods (Akram et al., 2014).
 69 Since hydraulic methods are usually computationally intensive, hydrologic methods are
 70 widely used all over the world. The unit hydrograph, proposed by Sherman (1932), is
 71 one of the methods most widely used in the development of flood prediction and
 72 warning systems for gauged basins with observed rainfall and runoff data (Singh et al.,
 73 2014). However, the UH method has inherent problems, such as areal lumping of
 74 catchment and rainfall characteristics as well as the utilization of linear system theory
 75 (Singh, 1988; James and Johanson, 1999). Moreover, current routing methods usually
 76 require numerous rainfall and runoff data. For watersheds with sparse gauging stations,
 77 it is difficult to develop an adequate relationship between physical watershed
 78 characteristics and unit hydrograph shape. The unit hydrograph estimation in small and
 79 ungauged basins is still a challenge in hydrological studies (Petroselli and Grimaldi,
 80 2015).

81 The UH, which is a surface runoff hydrograph resulting from one unit of rainfall
 82 excess uniformly distributed spatially and temporally over the watershed for the
 83 specified rainfall excess duration (Chow 1964), can be categorized into 4 major types
 84 (Singh, 1988), including traditional, probability-based, conceptual, and
 85 geomorphologic methods (Bhuyan et.al. 2015).

86 Synthetic UH methods establish the relationships between watershed
 87 characteristic for describing the UH, (e.g. peak flow, time to peak and time base) and

删除的内容: There are d

删除的内容: for the generation of runoff hydrograph

删除的内容: ,

删除的内容: and so on

删除的内容: the

删除的内容: and

删除的内容: the

删除的内容: U

删除的内容: H

删除的内容: (UH)

删除的内容: there are some

删除的内容: associated with the UH method

删除的内容: depends on

删除的内容: poor

删除的内容: parameters

删除的内容: the

删除的内容: critical issue

删除的内容: Flow routing is an important component in a hydrological model, whose accuracy directly affects flow forecasting. The Unit Hydrograph (UH), proposed by Sherman (1932), is one of the methods most widely used in the development of flood prediction and warning systems for gauged basins with observed rainfall-runoff data (Singh et al., 2014).

删除的内容: The traditional

删除的内容: between parameters used to describe the UH

114 parameters used to describe the basin. Snyder (1938), Mockus (1957) and U.S. Soil
115 Conservation Service (SCS) (2002) proposed some of these methods, which are still
116 used. The disadvantages of these methods are that they do not yield adequately
117 satisfactory results, and their application to practical engineering problems is tedious
118 and cumbersome (Nigussie et al., 2016).

删除的内容: traditional

119 Since most UHs have rising limbs steeper than their receding sides, and their shape
120 resembles typical probability distribution functions (PDFs), many PDFs have been used
121 for the derivation of UHs. The difficulty of this method is that the PDFs are diverse,
122 and their parameters depend on numerous hydrological data (Bhuyan et al., 2015).

123 Conceptual methods are another technique for deriving UHs. Nash (1957)
124 proposed a conceptual model composed of n linear reservoirs connected in series (or a
125 cascade) with the same storage coefficient K for the derivation of the instantaneous unit
126 hydrograph (IUH). Dooge (1959) proposed a generalized IUH based on linear
127 reservoirs, linear channels, and time-area concentration diagram. Bhunya et al. (2005)
128 and Singh et al. (2007) represented a hybrid method and an extended hybrid method
129 based on a linear reservoir. Singh (2015) proposed a new simple two-parameter IUH
130 with conceptual and physical justification. Khaleghi et al. (2018) suggested a new
131 conceptual model, namely, the inter-connected linear reservoir model (ICLRM) which,
132 however, neglects the impact of uneven basin surface on the UH.

133 Rodriguez-Iturbe (1979) proposed a geomorphologic instantaneous unit
134 hydrograph (GIUH) method, which couples the hydrologic characteristics of a

136 catchment with geomorphologic parameters (Singh, 1988; Kumar et al., 2007). In this
137 method, the IUH corresponds to the probability density function of travel times from
138 the locations of runoff production to the watershed outlet (Gupta et al., 1980; Singh,
139 1988). With the development of digital elevation models (DEMs) and geographic
140 information system (GIS) technology, the width function-based geomorphological IUH
141 method has been formulated. However, incapacity it is unable to properly account (i.e.
142 to respect the geometry) for the spatial distribution of rainfall (Rigon et al., 2016).

143 The UH method assumes the watershed response to be linear and time invariant,
144 and rainfall to be spatially homogeneous. Contrary to the linearity assumption, basins
145 have been shown to exhibit nonlinearity in the transformation of excess rainfall to
146 stormflow (Bunster et al., 2019). For a small watershed, Minshall (1960) showed that
147 significantly different UHs were produced by different rainfall intensities. To cope with
148 this nonlinearity, Rodríguez-Iturbe et al. (1982) extended the GIUH to the
149 geomorphoclimatic IUH (GcIUH) by incorporating excess rainfall intensity. Lee et al.
150 (2008) proposed a variable kinematic wave GIUH accounting for time-varying rainfall
151 intensity, which may be applicable to ungauged catchments that are influenced by high
152 intensity rainfall. Du et al. (2009) proposed a GIS based routing method to simulate
153 storm runoff with the consideration of spatial and temporal variability of runoff
154 generation and flow routing through hillslope and river network. A similar work was
155 done by Muzik (1996), Gironás et al. (2009), and Bunster et al. (2019).

156 The traditional, probabilistic, conceptual, and geomorphologic methods have not

157 been able to fully consider the geomorphic characteristics of the watershed and
158 incorporate time-varying rainfall intensity.

159 The spatially distributed unit hydrograph (DUH) method conceptualizes that the
160 unit hydrograph can be derived from the time-area curve of the watershed using the S-
161 curve method (Muzik, 1996). It is a type of geomorphoclimatic unit hydrograph, since
162 its derivation considers watershed geomorphology (Du et al., 2009), spatially
163 distributed flow celerity, and temporally varying excess rainfall intensities can be
164 considered in DUH (Bunster et al., 2019). In this method, the travel time of each grid
165 cell can be calculated by dividing the travel distance of a cell to the next cell by the
166 velocity of flow generated in that cell (Paul et al., 2018). The travel time is then summed
167 along the flow path to obtain the total travel time from each cell to the outlet. The DUH
168 is thus derived using the distribution of travel time from all grid cells in a watershed
169 (Bunster et al., 2019). Some DUH methods assumed a time-invariant travel time field
170 and ignored the dependence of travel time on excess rainfall intensity (Melesse &
171 Graham, 2004; Noto and La Loggia, 2007; Gibbs et al., 2010), while others suggested
172 various UHs corresponding to different storm events, namely time-varying distributed
173 unit hydrograph (TDUH) (Martinez et al., 2002; Sarangi et al., 2007; Du et al., 2009).
174 Compared to the fully distributed methods based on the momentum equation, the DUH
175 is a more efficient method because it allows for the use of distributed terrain information
176 and is an alternative to semi-distributed and fully distributed methods for rainfall-runoff
177 modelling (Bunster et al., 2019).

178 Besides excess rainfall intensity, the upstream contributions to the travel time
179 estimation have also been considered in the time-varying DUH method. For instance,
180 Maidment et al. (1996) defined the velocity in the cell as a function of the contributing
181 area to take into account the velocity increase observed downstream in river systems
182 (Gironás et al., 2009). Gad (2014) applied a grid-based method using stream power to
183 relate flow velocity to the hydrologic parameters of the upstream watershed area.
184 Similar work was done by Saghafian and Julien (1995), Bhattacharya et al. (2012) and
185 Chinh et al. (2013). A major drawback of this method is the assumption that the
186 watershed is near global equilibrium. Bunster et al. (2019) developed a spatially time-
187 varying DUH method that accounts for dynamic upstream contributions and
188 characterized the temporal behavior of upstream contributions and their impact on
189 travel times in the basin. However, this time-varying DUH also assumed that
190 equilibrium in each individual grid cell was reached before the end of the rainfall excess
191 pulse. When there accrues continuous excess-rainfall in a watershed, the soil moisture
192 content and surface runoff increase, and the infiltration rate decreases, leading to an
193 acceleration of flow routing velocity, until the entire basin is saturated and the routing
194 velocity reach its maximum. This assumption of equilibrium globally or in grid cells
195 yields faster travel flow velocities, smaller travel time, and higher peak discharge.
196 However, these approximations neglect the impact of dynamic changes of soil moisture
197 exchange and water storage in unsaturated regions.

198 The objective of this study was therefore to propose a time varying distributed unit

删除的内容: iswas

200 hydrograph method for runoff routing that accounts for dynamic rainfall intensity and
201 soil moisture content based on the Xinanjiang (XAJ) model, namely time-varying
202 distributed unit hydrograph considering soil moisture content (TDUH-MC). The main
203 contributions of the present study are as follows. First, a soil moisture content
204 proportional factor in the unsaturated area was identified and expressed based on the
205 Pareto distribution function. Second, the travel time function based on the kinematic
206 wave theory was modified by considering the soil moisture content proportional factor.
207 Besides rainfall intensity, the influence of time-varying soil moisture storage on flow
208 velocity in the watershed was considered, where runoff generation was dominated by
209 the saturation-excess mechanism. Finally, the Qin River basin and Longhu River basin
210 in the Guangdong Province, China, were selected as two case studies. The flow forecast
211 method mainly consisted of the calculation of excess rainfall and the derivation of DUH.
212 A new routing method was developed to incorporate the dynamic changes of soil
213 moisture content and rainfall intensity, and the XAJ model was adopted to calculate
214 excess rainfall. The SUH, DUH and TDUH methods were compared with the TDUH-
215 MC method, and sensitivity analysis of parameters was conducted.

删除的内容: proposed

216 2. Improvement of flow routing method

217 2.1 Calculation of flow velocity considering time-varying soil moisture 218 content

219 The DUH relies on the computation of travel time in the basin. Grimaldi et al.
220 (2010) found that the Soil Conservation Service (SCS) formula, given by Eq. (1), can

删除的内容: over a

223 be used to adequately define the basin flow time. This formula was also used by NRCS
224 (1997) and Grimaldi et al. (2012), but this formula is time invariant and the time-
225 varying rainfall intensity should be considered, ~~as given by Eq. (2), which was used by~~
226 Wong (1995), Muzik (1996), Bedient and Huber (2002), Gironas et al. (2009), Du et al.
227 (2009) and Kong et al. (2019).

删除的内容: which is

删除的内容: .

删除的内容: used this formula.

$$228 \quad V = k \cdot S^{\frac{1}{2}} \quad (1)$$

$$229 \quad V = k \cdot S^{\frac{1}{2}} \cdot \left(\frac{I_t}{I_c} \right)^{\frac{2}{5}} \quad (2)$$

230 where V (m/s) is the flow velocity; k (m/s) is ~~the~~ land use or flow type coefficient; S
231 (m/m) is the slope of the grid cell; I_t (mm/h) represents the excess rainfall intensity at
232 time t ; and I_c (mm/h) represents the reference excess rainfall intensity of the basin.

233 These formulas assume that equilibrium in individual grid cell can be reached
234 before the end of the rainfall excess (Bunster et al., 2019), which leads to larger flow
235 velocity, shorter travel time, and higher peak discharge. Actually, the hillslope flow
236 velocity in each grid is related to soil moisture content. Fast subsurface velocities and
237 quick runoff responses to precipitation have been observed on many hillslopes
238 (Hutchinson & Moore, 2000; Peters et al., 1995; Tani, 1997). The exact mechanisms
239 that cause water to move through the preferential flow path network are not well
240 quantified, but it is often assumed that saturated soil provides the connection between
241 preferential features (Sidle et al., 2001; Steenhuis et al., 1988). ~~Studies have also shown~~
242 that antecedent moisture condition, precipitation intensity, precipitation amount,

删除的内容: Many s

247 topography and so on play a significant role in flow configuration (Sidle et al., 2000;
248 Tsuboyama et al., 1994; Anderson et al., 2009).

删除的内容: this phenomenon

249 To that end, a soil moisture factor θ_t was introduced to characterize the soil
250 moisture content in unsaturated areas. Because the flow velocity will reach its
251 maximum value when the entire basin is saturated, this new factor (θ_t) was added to
252 the current time-varying flow velocity formula as

$$253 \quad V = k \cdot S^{\frac{1}{2}} \cdot \left(\frac{I_t}{I_c} \right)^{\frac{2}{5}} \cdot (\theta_t)^\gamma \quad (3)$$

254 where θ_t (unitless) represents the e the soil moisture content of unsaturated areas at
255 time t ; and γ (unitless) is an exponent smaller than unity, which represents the nonlinear
256 relationship between soil moisture content and flow velocity.

删除的内容: e state of

257 Factor θ_t was defined as the ratio of w_t and $w_{\max,t}$, which is expressed by

删除的内容: The f

$$258 \quad \theta_t = \frac{w_t}{w_{\max,t}} \quad (4)$$

259 where w_t (mm) represents the mean tension water storage of the unsaturated region; and
260 $w_{\max,t}$ (mm) represents the maximum tension water storage of the unsaturated region at
261 time t .

262 Specifically, w_t and $w_{\max,t}$ were calculated based on the Pareto distribution function
263 in this study. The Pareto distribution function has mostly been used to express the
264 spatial variability of soil moisture capacity (Moore, 1985). As shown in Fig. 1, the area
265 below the e curve represents the mean tension water capacity of the entire basin.

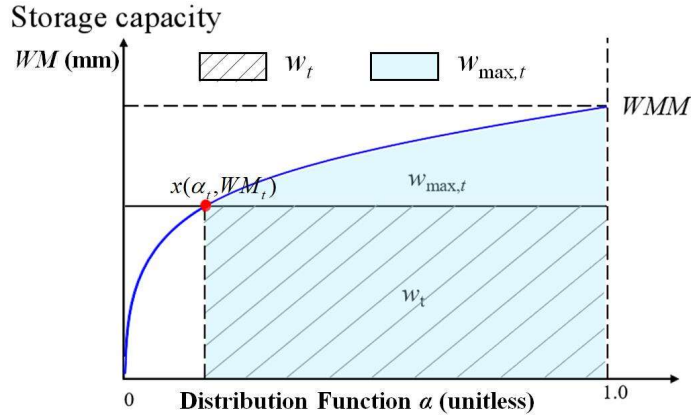
删除的内容: ,

删除的内容: which is

删除的内容: .

删除的内容: As shown in the figure,

删除的内容: is



274

275

Figure 1. Watershed storage capacity curve

276

For the tension water storage capacity curve, the specific formula is given by

277

$$\alpha = 1 - \left(1 - \frac{WM}{WMM}\right)^b \quad (5)$$

278

where α (unitless) represents the proportion of the basin area where the tension water

279

capacity is less than or equal to the value of the ordinate WM (mm). The tension water

280

capacity at a point, WM , varies from 0 to a maximum WMM (mm) according to Eq. (5).

281

Since the soil moisture content in a basin varies with time, the state of the

282

catchment at any time t can be represented by a point $x(\alpha_t, WM_t)$ on the curved line

283

of Fig. 1 (Zhao, 1992). The area to the right and below the point x is proportional to the

284

areal mean tension water storage (not capacity). Thus, WM_t , the ordinate of the point

285

x , represents the tension water storage capacity in the basin at time t ; w_t (mm) can be

286

assumed to represent the mean tension water storage of the unsaturated region, and

287

$w_{\max,t}$ (mm) represents the maximum tension water storage of the unsaturated region at

288

time t . Their expressions are given by

删除的内容: Actually,

删除的内容: .

删除的内容: T

292
$$\alpha_t = 1 - \left(1 - \frac{WM_t}{WMM}\right)^b \quad (6)$$

293
$$w_t = (1 - \alpha_t) \cdot WM_t \quad (7)$$

294
$$w_{\max,t} = \int_{\alpha_t}^1 WMM \left[1 - (1 - \alpha)^{\frac{1}{b}}\right] d\alpha \quad (8)$$

295 Combining Eqs. (4), (7), (8), the soil moisture content can be written as

296
$$\theta_t = \frac{w_t}{w_{\max,t}} = \frac{(1 - \alpha_t) \cdot WM_t}{\int_{\alpha_t}^1 WMM \left[1 - (1 - \alpha)^{\frac{1}{b}}\right] d\alpha} \quad (9)$$

297 Substituting Eq. (6) into Eq. (9),

298
$$\theta_t = \frac{(1 - \alpha_t) \cdot WM_t}{WMM \left[1 - \alpha_t - \frac{b}{b+1} (1 - \alpha_t)^{1 + \frac{1}{b}}\right]} = \frac{(b+1)WM_t}{WMM + bWM_t} \quad (10)$$

299 It can be seen from Eq. (10) that as rainfall continues, the soil moisture content in
 300 the unsaturated area continues to increase, whereas the non-runoff area continues to
 301 decrease. The range of θ_t is (0, 1], and with the gradual increase of soil moisture, θ_t
 302 tends to 1.

删除的内容: s

303 *2.2 Calculation of runoff routing based on DUH*

304 The GIS-derived DUH method was employed for runoff routing calculations,
 305 which allowed the velocity to be calculated on a grid cell basis over the watershed. The
 306 DUH routing method is a semi-analytical form of the width function-based IUH
 307 enumerated by Rigon et al. (2016). The DUH has been used for small ungauged basins.

309 To remove the linearity assumption, fully distributed models use routing methods which
310 are usually computationally intensive because they solve the St. Venant equations
311 (Bunster et al., 2019), so they are usually limited to small basins. Therefore, the DUH
312 method is an alternative method that allows the use of distributed information in a much
313 more efficient manner, and we applied it to different sizes of watersheds.

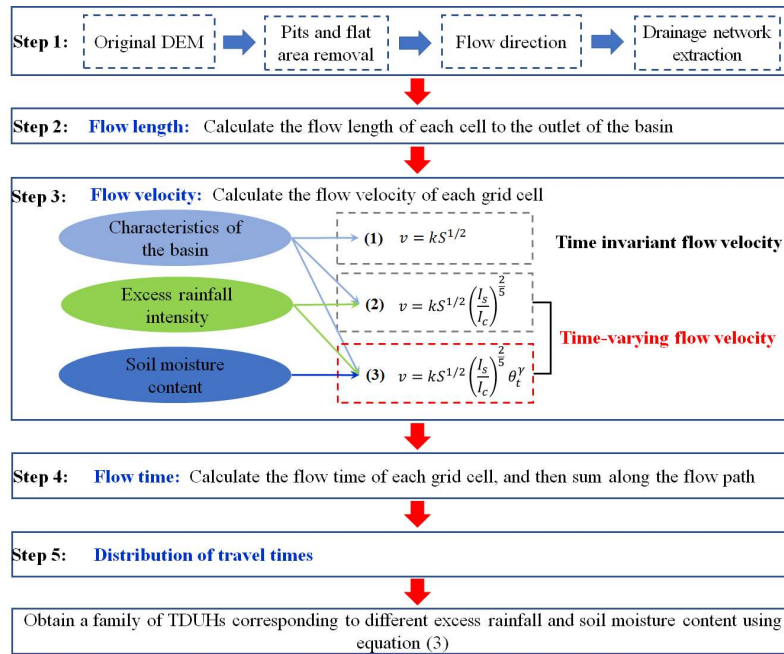
删除的内容: y

314 The core of the DUH method is to equate the probability density function of time
315 at which the rainfall flows to the basin outlet to form the instantaneous unit hydrograph,
316 in which the time-area relationship is derived using the velocity field with spatial
317 distribution characteristics. The traditional DUH method can route the time-variant
318 spatially distributed rainfall to the watershed outlet, but such a method is a lumped
319 linear model of watershed response (Grimaldi et al., 2010). The schematic diagram of
320 the DUH method is shown in Fig. 2.

删除的内容: of the basin

删除的内容: and

删除的内容: proposed DUH



325

326 **Figure 2.** Schematic diagram of the DUH method considering time-varying rainfall
 327 intensity and soil moisture content, in which Eqs. (1), (2) and (3) are the time invariant
 328 flow velocity, time-varying flow velocity considering excess rainfall intensity, and
 329 time-varying flow velocity considering both excess rainfall intensity and soil moisture
 330 content. The unit hydrograph derived from the three flow velocity equations correspond
 331 to DUH, TDUH and the TDUH-MC method respectively.

删除的内容: proposed

332 The steps of the DUH method are summarized as follows.

删除的内容: processes

333 1) The drainage network based on the advanced DEM pre-processing method is
 334 identified. More details can be found in Grimaldi et al. (2012).

删除的内容: using

删除的内容: techniques

335 2) Estimate the flow path, which is measured for each grid cell along the flow
 336 directions to the basin outlet.

删除的内容: of basins

342 3) Calculate the flow velocity based on watershed characteristics of the and the
343 spatial temporal distribution characteristics of rainfall. Several flow velocity formulas
344 are commonly used for deriving the spatially distributed unit hydrograph, such as
345 Manning' formula (Chow et al., 1988), SCS formula (Haan et al., 1994), Darcy-
346 Weisbach formula (Katz et al., 1995), and Maidment et al. (1996) uniform flow
347 equation.

- 删除的内容: the
- 删除的内容: watershed
- 删除的内容: -
- 删除的内容: the

348 4) To compute the total travel time τ_i of flow from each cell i to the outlet, we
349 added travel times along the R_i cells belonging to the flow path that starts at that cell,
350 given by Eq. (11) (Muzik, 1996). The travel time for each grid cell can be calculated by
351 Eq. (12):

- 删除的内容: using

352
$$\tau_i = \sum_{i \in R_i} \Delta \tau_i \quad (11)$$

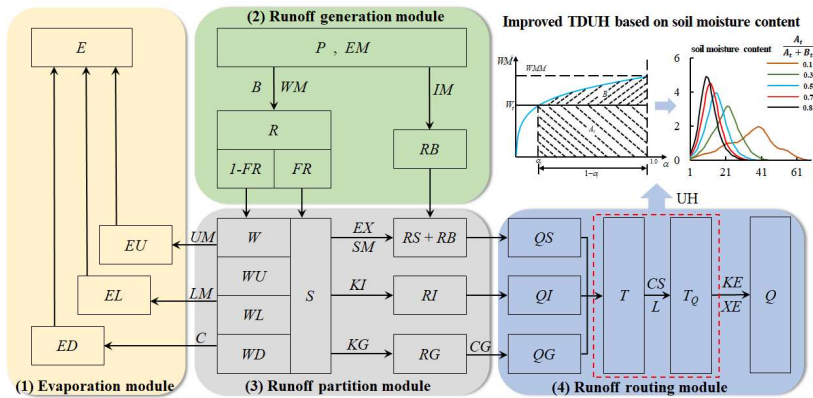
353
$$\Delta \tau_i = \frac{L_i}{V} \quad \text{or} \quad \Delta \tau_i = \frac{\sqrt{2}L_i}{V} \quad (12)$$

354 where $\Delta \tau_i$ is the retention time in grid cell i ; τ_i is the total travel time along the flow
355 path in grid cell i ; L_i is the grid cell size; travel length in a specific grid cell is the cell
356 size L_i when the rasterized flow is flowing along the edges of the grid, whereas the
357 travel length is $\sqrt{2}L_i$ when it is flowing diagonally.

358 5) Develop a cumulative travel time map of the watershed based on cell by cell
359 estimates for hillslope velocities. The cumulative travel time map is further divided into
360 isochrones, which can be used to generate a time-area curve and the resulting unit
361 hydrograph (Kilgore, 1997).

367 **3. Calculation of runoff generation**

368 The Xinanjiang (XAJ) model was used for the calculation of excess rainfall in this
 369 study. It is a conceptual hydrologic model proposed by Zhao et al. (1980) for flood
 370 forecasts in the Xinan River basin. The XAJ model has been widely used in humid and
 371 semi-humid watersheds all over the world (Zhao, 1992). It mainly consists of four
 372 modules, namely evapotranspiration module, runoff generation module, runoff partition
 373 module and runoff routing module (Zhou et al., 2019). Usually, a large watershed is
 374 divided into several sub-basins to capture the spatial variability of underlying surface,
 375 precipitation, and evaporation. In each sub-basin, the inputs of the XAJ model are the
 376 average areal rainfall as well as evaporation, and the output is streamflow. The
 377 schematic diagram of the XAJ model is shown in Fig. 3.



378
 379 **Figure 3.** Schematic diagram of the XAJ model

380 First, for the evapotranspiration module, the soil profile of each sub-basin is
 381 divided into three layers, the upper, lower and deeper layers, and only when water in
 382 the layer above it has been exhausted, evaporation from the next layer occurs. Second,

删除的内容: water

384 for runoff generation in the XAJ model, a catchment is divided into two parts by the
385 percentage of impervious and saturated areas, namely pervious and impervious areas,
386 respectively. Since the soil moisture deficit is heterogeneous, runoff distribution is
387 usually nonuniform across the basin. Thus, a storage capacity curve was adopted by the
388 XAJ model to accommodate the nonuniformity of soil moisture deficit or the tension
389 water capacity distribution. Third, the runoff partition in the XAJ model divides the
390 total runoff into three components by a free reservoir, which consists of surface runoff
391 (RS), interflow runoff (RI), and groundwater runoff (RG). More details can be found in
392 (Zhao et al., 1980).

删除的内容: as

删除的内容: permeable

393 Finally, the SUH was selected as runoff routing approach in the XAJ model.
394 Specifically, the Nash instantaneous unit hydrograph model (Nash, 1957) was used to
395 derive the SUH in this study. For the Nash IUH model, a catchment was assumed to be
396 made up of a series of n identical linear reservoirs, each with the same storage constant
397 K . The magnitudes of n and K were estimated based on the observed excess rainfall
398 hydrograph and corresponding direct runoff hydrograph using the method of moments.
399 Details can be found in Singh (1988) and Chow et al. (1988).

带格式的: 缩进: 首行缩进: 2 字符

带格式的: 字体: 倾斜

带格式的: 字体: 倾斜

带格式的: 字体: 倾斜

带格式的: 字体: 倾斜

删除的内容: .

Finally, the SUH, DUH, TDUH and the method were used to calculate flow routing, respectively. .

删除的内容: was withswere. he details can be found in Singh (1988) and Chow et al. (1988) .

删除的内容: Maskingen

删除的内容: catchment

删除的内容: is

删除的内容: (

带格式的: 字体: 倾斜

删除的内容:)

带格式的: 字体: 倾斜

400 The Muskingum method was employed to produce streamflow from each sub-
401 basin to the outlet of the entire basin. For the SUH, the basin was taken as a whole. The
402 parameters of the Muskingum method, including the Muskingum time constant KE and
403 Muskingum weighting factor XE , were calibrated with those of the XAJ model. The
404 SCE-UA method was used to calibrate the parameters of XAJ model (Chu et al., 2009;

417 Moghaddam et al., 2016). For the DUH, the basin was divided into several sub-basins.
 418 Since natural rivers are multiple inflow-single outflow runoff systems with different
 419 travel times from the sub-basins to the outlet, we adopted the physical-numerical
 420 principles established by Cunge to calculate the routing parameters of the Muskingum
 421 method, which is suitable for ungauged watersheds (Ponce et al., 1996). The
 422 Muskingum parameters for each sub-basin were determined based on flow and channel
 423 characteristics, such as the top width of the river, wave celerity, reach length and reach
 424 slope, as described in Chow (1959) and Wilson and Ruffin (1988).

425 **4. Study area and data**

426 The Qin River basin and Longhu River basin were selected as two case study
 427 watersheds. One is a large watershed, and the other is a small watershed. The
 428 applicability of the TDUH-MC method to different size watersheds was verified, and
 429 parameter sensitivity analysis was done to evaluate the performance of the TDUH-MC
 430 method (Chen et al., 2022).

431 The Qin River is a tributary of the Mei River, which originates from Guangdong
 432 Province, China. The river is 91 km long with a basin area of 1578 km². The mean slope
 433 of the basin is 1.1‰. There are 21 meteorological stations and 1 flow station (the
 434 Jianshan Station) in the basin, as shown in Fig. 4. Using the DEM data of the Qin River
 435 basin, the whole basin was divided into 9 sub-basins, namely Sub-basins 1-9 from

删除的内容: any

删除的内容: is

删除的内容: s

删除的内容: to be applied to

删除的内容: parameters of the

删除的内容: method

删除的内容: which can be found

删除的内容: (

删除的内容: , 1959;

删除的内容: ,

删除的内容: proposed

删除的内容: proposed

删除的内容: this

删除的内容: area

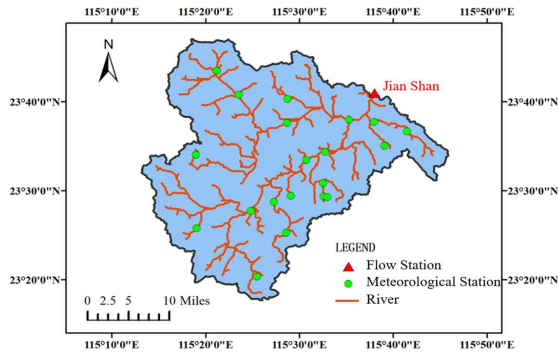
删除的内容: ,

删除的内容:

删除的内容: based on the natural water system,

删除的内容: s

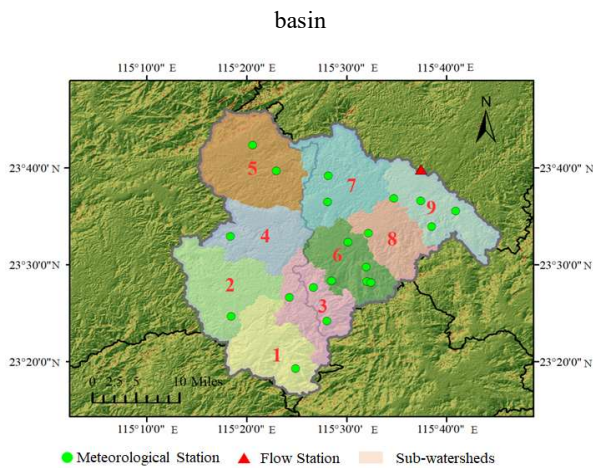
454 upstream to downstream as shown in Fig. 5. Details of each sub-basin are given in Table
 455 1.



456
 457 **Figure 4.** Locations of meteorological stations and flow stations in the Qin River

删除的内容: Distribution diagram

458



459
 460 **Figure 5.** Sub-basins of the Qin River basin (*Note.* The satellite images for the study

删除的内容: .

461

area are available at <http://www.gscloud.cn>)

462

Table 1. Detailed information of each sub-basin.

Sub-basins	Drainage area/km ²	Number of grids	Average slope	<i>KE</i>	<i>XE</i>
Sub-basin 1	175.64	176	13.29	<u>10.7</u>	<u>0.13</u>
Sub-basin 2	195.86	197	9.27	<u>10.7</u>	<u>0.13</u>

删除的内容: l

删除的内容: on

带格式的: 字体: 非加粗

删除的内容: s

Sub-basin 3	154.97	156	12.50	<u>8.3</u>	<u>0.12</u>
Sub-basin 4	153.08	151	9.57	<u>5.9</u>	<u>0.15</u>
Sub-basin 5	147.79	147	12.49	<u>5.9</u>	<u>0.15</u>
Sub-basin 6	249.36	253	11.74	<u>4.7</u>	<u>0.11</u>
Sub-basin 7	213.34	211	10.56	<u>2.1</u>	<u>0.11</u>
Sub-basin 8	122.28	129	10.77	<u>2.1</u>	<u>0.11</u>
Sub-basin 9	166.51	161	9.74	<u>/</u>	<u>/</u>

468 The Longhu River basin is a small watershed, which has a drainage area of 102.7
469 km², located in the Guangdong Province, China. The length of the River is 17.4 km.

470 The rainfall and evaporation data from meteorological stations for the two basins
471 was collected from 1959 to 2018, and the simultaneous hourly runoff data for the
472 Jianshan Station and Longhu Station was collected as well. A total of 64 isolated storms
473 with the observed runoff responses from 1959 to 2018 were selected to calibrate and
474 verify the established model, of which 35 events were collected from the Qin River
475 basin and 29 from the Longhu River basin. 25 and 23 flow events were used for model
476 calibration in the Qin and Longhu River basins respectively, and 10 and 6 flow events
477 were used for model validation in the two basins.

478 The statistics of flow events used for model calibration and validation are shown
479 in Fig. 6. The average peak flows of the two basins were 1311 m³/s and 118 m³/s, and
480 the average flood durations were about 50 h and 13 h, respectively. The antecedent
481 precipitation was calculated, based on the daily recession coefficient of water storage
482 in the basin.

删除的内容: for the two basins

删除的内容:

删除的内容: The simultaneous hourly runoff data for the Jianshan Station and Longhu Station was collected as well.

删除的内容: od

删除的内容: flow

删除的内容: statistics

删除的内容: are

删除的内容: are

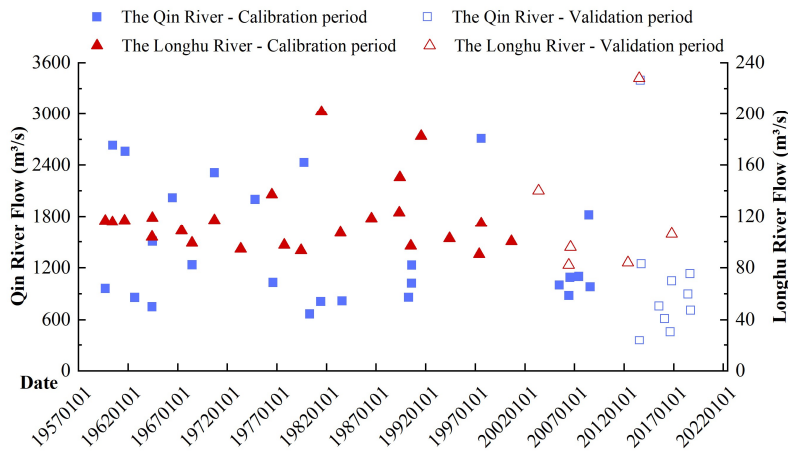


Figure 6. Statistics of flow events used for model calibration and validation

5. Results and discussion

5.1 Calibration of parameters

5.1.1 Model calibration

The runoff generation model (XAJ model) and the routing model were calibrated separately in this study. First, the SUH and several distributed unit hydrographs (DUH, TDUH and MC-TDUH) were derived. Second, the Shuffled Complex Evolution Algorithm (SCE-UA) method, developed by the University of Arizona (Duan et al., 1992), was used to optimize the XAJ model parameters (Vrugt et al., 2006; Beskow et al., 2011; Zhou et al., 2018). The SUH was selected as the runoff routing method. As the SUH was derived from observed rainfall and runoff, the flow routing model corrected some inconsistencies of the hydrological model. Therefore, the parameters of excess runoff were calibrated. Third, the performances of XAJ+ SUH and XAJ+DUHs

带格式的： 缩进： 首行缩进： 0 字符

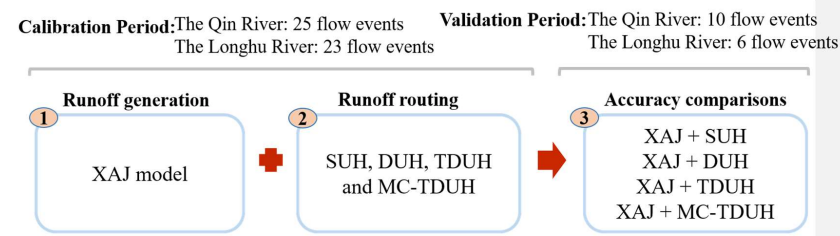
删除的内容： Flow event

删除的内容： s

删除的内容： od

删除的内容： s

510 (DUH, TDUH and MC-TDUH) were compared. Since the XAJ model parameters were
 511 determined by combining with SUH routing method, this calibration method would be
 512 more inclined to optimize the performance of XAJ + SUH model. When combined with
 513 other confluence models, the accuracy of results may be affected to some extent. The
 514 schematic of the calibration procedure is given below.



515
 516 **Figure 7. Schematic of the calibration procedure**

517 The steps of parameter calibration can be summarized as follows:

518 1) The XAJ model was used to calculate the excess rainfall, in which, the SUH
 519 derived from observed runoff was selected as the runoff routing method. The SCE-UA
 520 method was used to optimize the XAJ model parameters in this study. 25 and 23 flow
 521 events in the Qin River basin and Longhu River basin were used for the calibration of
 522 the XAJ + SUH model.

523 2) The SUH was derived using 25 and 23 flow events in the Qin River basin and
 524 Longhu River basin, respectively. The DUH, TDUH and MC-TDUH were derived,
 525 based on physical characteristics and rainfall intensities of the watersheds. The
 526 parameters determination method is given in Section 5.1.3.

527 3) Since the objective of this study was to propose a new flow routing method, the
 528 runoff production model with its parameters were not changed in order to discuss the
 529 performance of flow routing models. The XAJ model with calibrated parameters in Step
 530 1) and DUH, TDUH as well as MC-TDUH determined in Step 2) were used for the
 531 validation period. 10 and 6 flow events of the two basins were then used for the
 532 validation of the XAJ + (SUH, DUH, TDUH and MC-TDUH) model.

533 The Nash-Sutcliffe efficiency (E_{NS}) (Nash and Sutcliffe, 1970; Chen et al., 2015),
 534 the Kling-Gupta efficiency (E_{KG}) (Gupta et al., 2009), and the root-mean-squared error
 535 to standard deviation ratio (R_{SR}) were chosen as criteria. Moreover, the new aggregated
 536 objective function (Brunner et al., 2021) targeted at optimizing flow characteristics was
 537 composed of these three metrics, in which E_{KG} focuses on high flows (Mizukami et al.,
 538 2019), $\log(E_{NS})$ emphasizes low flows, and R_{SR} quantifies volume errors. Similar
 539 method has been used by (Chen et al., 2022a; Chen et al., 2022b). Three metrics and
 540 the aggregated objective function are expressed by

$$541 \quad E_{NS} = 1 - \frac{\sum_{t=1}^T |Q_s^t - Q_o^t|}{\sum_{t=1}^T |Q_o^t - \bar{Q}_o|} \quad (13)$$

$$542 \quad E_{KG} = 1 - \sqrt{(r-1)^2 + \left(\frac{\sigma_s}{\sigma_o} - 1\right)^2 + \left(\frac{\mu_s}{\mu_o} - 1\right)^2} \quad (14)$$

$$543 \quad R_{SR} = \sqrt{\frac{\sum_{t=1}^T (Q_o^t - Q_s^t)^2}{\sum_{t=1}^T (Q_o^t - \bar{Q}_o)^2}} \quad (15)$$

$$544 \quad M = 0.5 \times (1 - E_{NS}) + 0.25 \times (1 - E_{KG}) + 0.15 \times (1 - \log(E_{NS})) + 0.1 \times R_{SR} \quad (16)$$

删除的内容:

The SCE-UA (Shuffled Complex Evolution Algorithm) method, developed by the University of Arizona in 1992 (Duan et al., 1992), is suitable for nonlinear, high dimension optimization problems. The method has been widely used for the calibration of hydrological models (Vrugt et al., 2006; Beskow et al., 2011; Zhou et al., 2018). Hence, the SCE-UA method was used to optimize the parameters of XAJ model in this study.

554 where Q_o^t is the observed discharge at time t ; Q_s^t is the simulated discharge at time
555 t ; \bar{Q}_o is the mean of observed discharge; T is the duration of the flow event; r is the
556 correlation coefficient between observed and simulated floods; σ_s and σ_o are the
557 standard deviation values for the simulated and observed responses, respectively; and
558 μ_s and μ_o are the corresponding mean values.

删除的内容: od

删除的内容: the

559 5.1.2 Calibrated parameters of runoff generation using the XAJ Model

560 Since the Qin River basin and Longhu River basin are in a humid area of southern
561 China, the saturation-excess mechanism with three-source runoff separation of the XAJ
562 model was adopted to calculate excess rainfall. The initial condition of the XAJ model
563 was considered by calculating the antecedent precipitation index before each flow event
564 (Linsley et al. 1949). The synthetic unit hydrograph, derived by historical rainfall-
565 runoff data, was used for flow routing in the process of model calibration. The time
566 interval was 1 hour. Several studies have shown that UH which is derived by
567 considering antecedent soil moisture is more consistent than UH which ignores that
568 (Yue and Hashino, 2000; Nourani et al., 2009). Therefore, the antecedent precipitation
569 was calculated and considered in this study. In order to obtain the SUH, we defined
570 excess rainfall and separated direct runoff and baseflow hydrographs in advance. The
571 final SUH used for calibration is the average value deduced by multiple historical flow
572 events. The parameters n of the Qin River basin and Longhu River basin was 4 and 3,
573 and the parameters K for the two basins was 3.4 and 2.1, respectively. Then, the flow

删除的内容: the

删除的内容: method

删除的内容: the

删除的内容: flow

删除的内容: od

删除的内容: (flood event 统一)

带格式的: 突出显示

删除的内容: The initial condition of the XAJ model was considered by calculating the antecedent precipitation index before each flow event (Linsley et al. 1949). In addition, the parameters of the XAJ model and the proposed distributed unit hydrograph were calibrated separately. Since the objective of this study is was to propose a new flow routing method, the runoff producing model with its parameters were not changed in order to discuss the performance of the flow routing models.

删除的内容: was

删除的内容: The

593 peak, flow volume, and the occurrence time of flow peak are three main basic elements
 594 for describing the flow hydrograph, and Eq. (16) was used as the aggregated objective
 595 function. The average Nash-Sutcliffe efficiency, relative flood peak error, and peak
 596 occurrence time error obtained in the calibration period of the XAJ model were 0.84,
 597 10.4%, and 4.96 hours, respectively, for the Qin River basin. Accordingly, for the
 598 Longhu River basin, it was 0.86, 8.81%, and 2.75 hours respectively, indicating a good
 599 performance of the XAJ model. Detailed information on the calibrated parameters of
 600 the XAJ model is shown in Table 2.

删除的内容: are

删除的内容: is

601 **Table 2.** Calibrated parameters of the XAJ model

Parameters	Physical meaning	The Qin River	The Longhu River	Unit
<i>UM</i>	Averaged soil moisture storage capacity of the upper layer	20.05	8.24	mm
<i>LM</i>	Averaged soil moisture storage capacity of the lower layer	74.42	72.98	mm
<i>DM</i>	Averaged soil moisture storage capacity of the deep layer	26.54	22.30	mm
<i>B</i>	Exponential of distribution of tension water capacity	0.25	0.12	-
<i>IM</i>	Ratio of impervious to total areas in the catchment	0.01	0.01	-
<i>K</i>	Ratio of potential evapotranspiration to pan evaporation	0.85	0.89	-
<i>C</i>	Evapotranspiration coefficient of the deeper layer	0.15	0.12	-
<i>SM</i>	Free water capacity of the surface layer	45.32	50.23	mm
<i>EX</i>	Exponent of the free water capacity curve influencing the development of the saturated area	1.50	1.50	-
<i>KI</i>	Outflow coefficient of free water storage to interflow	0.38	0.13	-
<i>KG</i>	Outflow coefficient of free water storage to groundwater	0.26	0.65	-
<i>CI</i>	Recession constant of the lower interflow storage	0.85	0.83	-
<i>CG</i>	Recession constant of the ground water storage	0.99	0.99	-
<i>CS</i>	Recession constant in the lag and rout method for routing through the channel system within each sub-	0.46	0.7	-

	basin			
KE	Muskingum time constant for each sub-reach	22.80	3.5	-
XE	Muskingum weighting factor for each sub-reach	0.13	0.12	-

604 5.1.3 Calibrated Parameters of the TDUH-MC flow routing method

605 As mentioned in Section 2.2, the core of the DUH is the calculation of the grid
606 flow velocity. As shown in Eq. (3), the parameters that needed to be calibrated were k ,
607 S , I_c and γ , in which I_c was determined using hourly mean rainfall intensity and flow
608 forecast of the target basin. For the Qin River basin, I_c was set at 20 mm/h, because the
609 mean rainfall intensity of multiple flows was about 20mm/h, and this parameter was 10
610 mm/h for the Longhu River basin. Additionally, parameter γ reflected the influence
611 of soil moisture content in unsaturated regions on flow velocity. The smaller the
612 parameter γ was, the smaller the influence of soil moisture content on the flow
613 velocity was. When the value of γ was equal to 1, the flow velocity of grid cell was
614 proportional to the soil moisture content factor θ_i . The parameter γ of soil moisture
615 content was determined to be 0.5 to reflect the influence of soil moisture content on the
616 flow velocity for the two basins. Furthermore, sensitivity analysis for this parameter
617 was conducted in Section 5.6. In order to get the grid cell slope S , the slope distribution
618 of the study areas was obtained from the DEM data of the target basin. Fig. 8(a) plots
619 the slope distribution of the Qin River basin. Parameter k is the velocity coefficient,
620 which was determined, based on different underlying surface types or different flow
621 states (Ajward & Muzik, 2000). Parameter k changed with different land types, and the
622 k values used in this study are given in Table 3. The land types of the Qin River basin

删除的内容:分节符(下一页).....

删除的内容: *proposed*

删除的内容: are

删除的内容: K

删除的内容: can be

删除的内容: 6

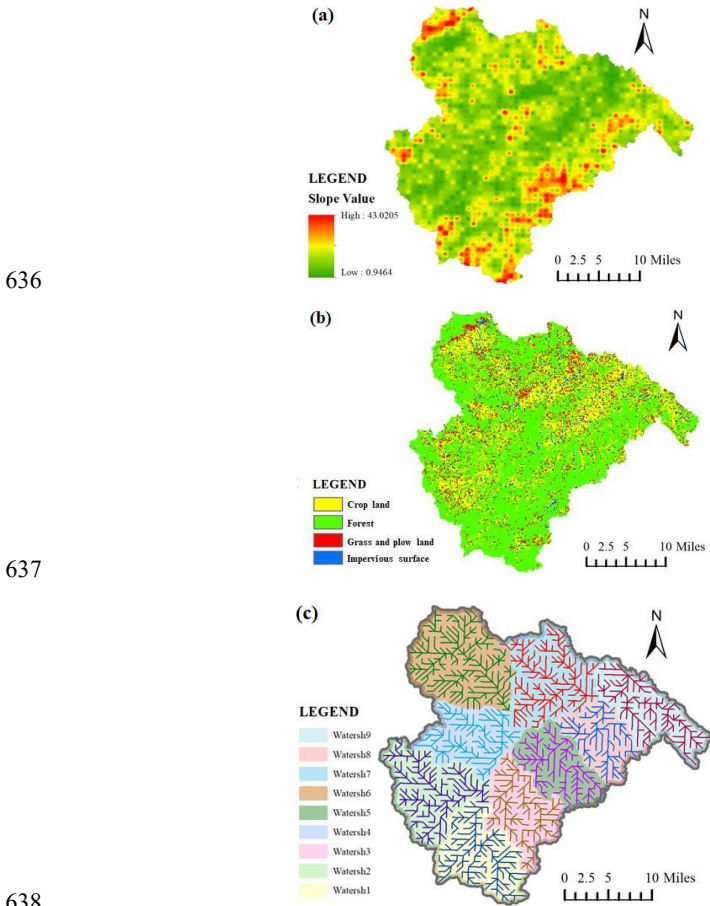
删除的内容: 7

删除的内容: The p

删除的内容: The p

删除的内容: s

634 are shown in Fig. 8(b). Then the k values of each grid cell were determined by
 635 combining Fig. 8(b) and Table 3.



638 **Figure 8.** Slope, Land types and rasterized flow direction of the Qin River basin

640 (a) Slope distribution. (b) Land types. (c) Rasterized flow direction.

641 **Table 3.** Specific values of k for different vegetational types

删除的内容: 6

删除的内容: 7

删除的内容: 6

删除的内容: 7

带格式的: 字体: 非倾斜

删除的内容: 6

删除的内容: 7

删除的内容: Land

Land type	Vegetational form	k (m/s)
Crop land	Fallow	1.37
	Contour tillage	1.40
	Straight plough	2.77
Grass and plow land	Trample	0.30
	Lush	0.46
	Sparse	0.64
	Pasture	0.40
Forest	Dense	0.21
	Sparse	0.43
	Full of dead leaves	0.76
Impervious surface	\	6.22

649 The grid flow velocity was calculated by Eq. (3) with the above parameter values.

650 Then, the flow travel time was determined by Eq. (11) and Eq. (12). It is noteworthy

651 that the raster size of the Qin River basin was divided into 1km×1km, and the rasterized

652 flow direction of each sub-basin is shown in Fig. 8(c). For the Longhu River basin, the

653 difference was that its cell size was divided into 30m×30m to evaluate the performance

654 of the TDUH-MC method in this small watershed.

655 5.2 Calculation of the TDUH-MC

656 After determining the parameters, flow routing was calculated, based on the

657 proposed DUH considering the time-varying soil moisture content. In order to improve

658 the effectiveness of the routing method, the rainfall intensity and soil moisture content

659 parameters were discretized. Then, a simplified TDUH considering time-varying soil

660 moisture content and TDUH were obtained in a certain range of rainfall intensities or

删除的内容: nasin

删除的内容: 6

删除的内容: 7

删除的内容: proposed

删除的内容: proposed time-varying DUH

删除的内容: above

删除的内容: efficiency and

668 soil moisture contents; these ranges are presented in Tables 4 and 5. To evaluate the
 669 performance of the TDUH-MC method, the traditional SUH, DUH and TDUH methods
 670 were used for comparison.

删除的内容: proposed

删除的内容: s

671 **Table 4.** The ratio of I_t to I_c of each period corresponds to the discrete rain intensity I_s

I_t / I_c (mm/h)	$0 < \frac{I_t}{I_c} \leq 0.5$	$0.5 < \frac{I_t}{I_c} \leq 1$	$1 < \frac{I_t}{I_c} \leq 1.5$	$\frac{I_t}{I_c} > 1.5$
Discrete I_s (mm/h)	0.5	1	1.5	2

672 **Table 5.** The soil moisture content θ_t of each period corresponds to the discrete soil
 673 moisture content θ_s

Soil moisture content θ_t	$0 < \theta_t \leq 0.2$	$0.2 < \theta_t \leq 0.4$	$0.4 < \theta_t \leq 0.6$	$0.6 < \theta_t \leq 0.8$	$\theta_t > 0.8$
Discrete soil moisture content θ_s	0.1	0.3	0.5	0.7	0.85

带格式表格

674 The DUH without considering rainfall intensity and soil moisture was obtained
 675 using Eq. (1). Results of the DUH for each sub-basin of the Qin River basin are shown
 676 in Fig. 9. There is only one DUH for a specific sub-basin due to the simplification of
 677 the underlying surface, such as slope and land covers. The differences among the DUHs
 678 were mainly reflected in flow peaks and their occurrence times. It can be also seen from
 679 Fig. 9 that the peak of DUHs in sub-basins 4 and 6 were significantly lower than in
 680 others. The reason may be that the smaller mean slope values of sub-basins 4 and 6 lead
 681 to lower flow velocity, resulting in lower peak of the DUH.

删除的内容: 7

删除的内容: 7

删除的内容: 6

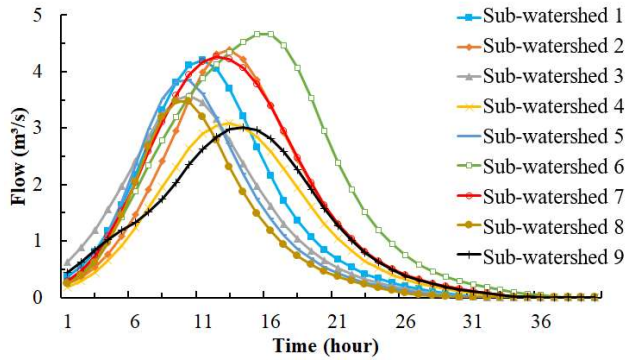


Figure 9. DUH for the Qin River basin

删除的内容: 7

The TDUHs corresponding to different rainfall intensities of 9 sub-basins are shown in Fig. 10. It can be seen from Fig. 10 that different rainfall intensities corresponded to different TDUHs. The increased rainfall intensity led to higher peak and earlier peak occurrence time of the UH. This is because that a larger rainfall intensity caused a larger flow velocity according to Eq. (2). In the practical use of TDUH, the UHs need to be selected according to rainfall intensities.

删除的内容: 8

删除的内容: 8

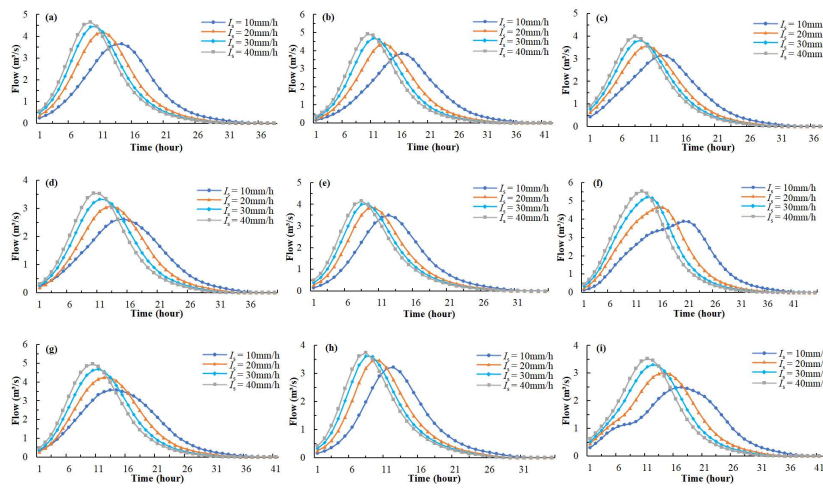
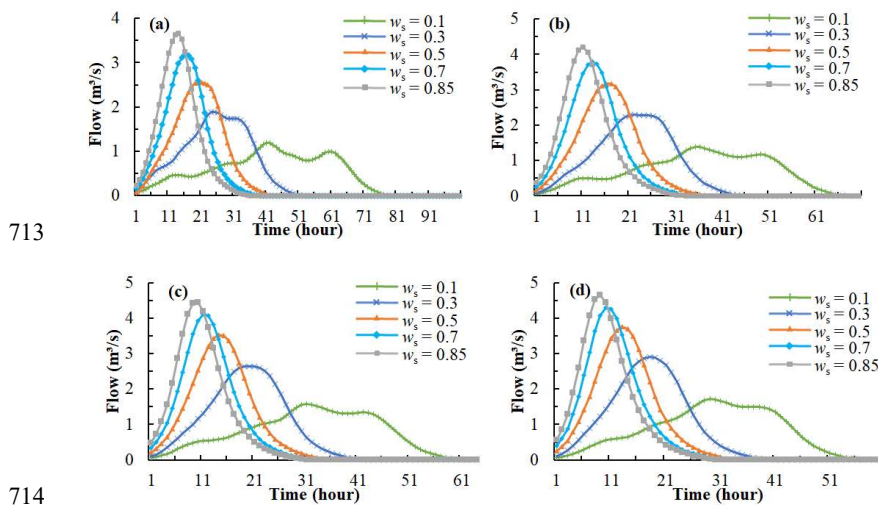


Figure 10. The TDUH for the Qin River basin. (a) Sub-basin 1. (b) Sub-basin 2. (c)

删除的内容: 8

703 Sub-basin 3. (d) Sub-basin 4. (e) Sub-basin 5. (f) Sub-basin 6. (g) Sub-basin 7. (h) Sub-
 704 basin 8. (i) Sub-basin 9.

705 The TDUH of each sub-basin was further divided according to the soil moisture
 706 content. The TDUHs considering soil moisture contents of sub-basin 1 are shown in
 707 Fig. 11. Obviously, under the same rainfall intensity, the soil moisture content was of
 708 great importance to the shape, peak value and duration of the TDUH. Specifically, when
 709 the proportion of soil moisture content θ_t increased, the TDUH-MC method
 710 considering soil moisture content was accompanied by steeper rising limb, higher peak
 711 and shorter duration. After the whole basin was saturated, the TDUH considering the
 712 soil moisture content was the same as the TDUH.



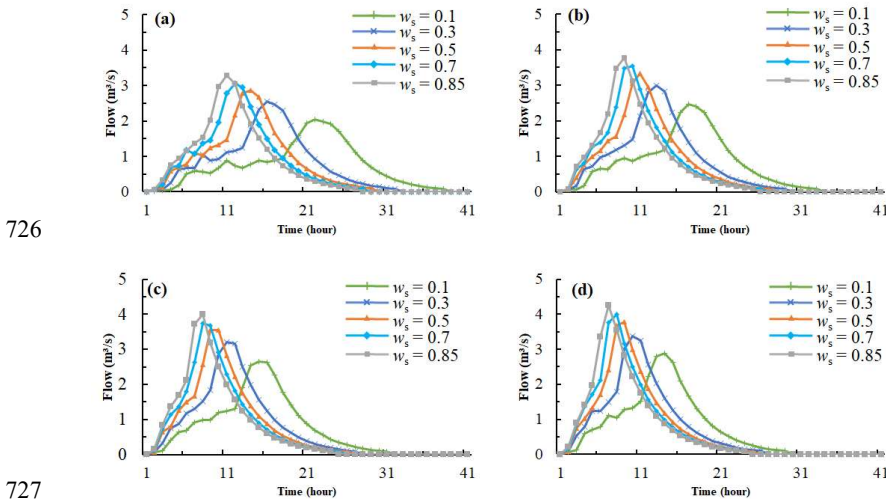
713
 714
 715 **Figure 11.** The TDUH considering soil moisture content for sub-basin 1 of the Qin
 716 River basin. (a) $I_s=0.5$. (b) $I_s=1$. (c) $I_s=1.5$. (d) $I_s=2$.

717 Similarly, the TDUHs considering the soil moisture content for the Longhu River

删除的内容: 9
 删除的内容: 0
 删除的内容: proposed

删除的内容: 9
 删除的内容: 0

723 basin are shown in Fig. 12. The grey line in Fig. 12(b) is the DUH, where I_s is equal
 724 to 1 and w_s is 0.85. Four grey unit hydrographs in Fig. 12(a) to 12(d) make up the
 725 TDUH without considering the soil moisture content.



726
 727
 728 **Figure 12.** The TDUH considering soil moisture content for the Longhu River basin.
 729 (a) $I_s = 0.5$. (b) $I_s = 1$. (c) $I_s = 1.5$. (d) $I_s = 2$.

730 5.3 Comparisons of flood routing methods

731 The runoff generation module of the calibrated XAJ model was used to calculate
 732 the excess rainfall, and the SUH, DUH, TDUH and improved TDUH considering soil
 733 moisture content were employed for flow routing calculations, respectively. The
 734 Muskingum parameters for each sub-basin are given in Table 1. Dozens of flow events
 735 were applied for model validation. Simulated results of the four methods for the Qin
 736 River basin are shown in Table 6. Three criteria were used for model performance

删除的内容: 0
 删除的内容: 0
 删除的内容: 10
 删除的内容: 1
 删除的内容: 10
 删除的内容: 1

删除的内容: 10
 删除的内容: 1

删除的内容:

746 evaluation, which included the Nash-Sutcliffe efficiency (E_{NS}), the ratio between the
 747 simulated and observed peak discharges (Q_p^s / Q_p^o), and the error between simulated and
 748 observed times to peak ($|t_p^s - t_p^o|$). The ratio between simulated and observed peak
 749 discharges of the TDUH-MC method ranged from 0.97 to 1.10. The average peak
 750 occurrence time error of the TDUH-MC method was 1.4h, which was the smallest
 751 among the four methods, and the mean E_{NS} coefficients of the ten flow events for
 752 validation were above 0.8. Fig. 13 shows the flow hydrographs of the four routing
 753 methods for part of the flow events (Event No. 20130720, 20130817, 20150709,
 754 20160128, 20161021 and 20180916). It is demonstrated that the TDUH-MC method
 755 outperformed the remaining three routing methods.

756 In addition, the forecast results of six flow events in the Longhu River basin using
 757 the SUH, DUT, TDUH and the TDUH-MC method are presented in Table 7. Results of
 758 the TDUH-MC method generally showed the best performance, which also verified the
 759 TDUH-MC formula for the small watershed. In general, the TDUH-MC method did
 760 better simulation in this watershed than in the Qin River basin.

761 **Table 6.** Comparison of four routing methods for the Qin River basin

Event number	$(Q_p^s / Q_p^o) / (t_p^s - t_p^o) / (E_{NS})$			
	SUH	DUH	TDUH	<u>TDUH-MC</u>
20130720	1.16/1/0.44	1.13/3/0.32	1.13/3/0.31	1.02/1/0.64
20130817	1.06/3/0.86	1.04/7/0.61	1.01/4/0.92	0.99/1/0.98
20130922	0.95/2/0.82	1.07/3/0.82	1.04/2/0.87	0.98/3/0.85
20150709	0.83/0/0.80	1.01/2/0.87	1.26/2/0.63	1.07/1/0.97
20160128	0.89/2/0.93	1.09/3/0.74	0.93/1/0.83	1.01/0/0.97
20160827	1.14/3/0.83	1.10/2/0.75	1.12/2/0.81	1.07/1/0.91

删除的内容: proposed

删除的内容: proposed

删除的内容: 11

删除的内容: 2

删除的内容: proposed

删除的内容: proposed

删除的内容: proposed

删除的内容: proposed

删除的内容: in

删除的内容: proposed

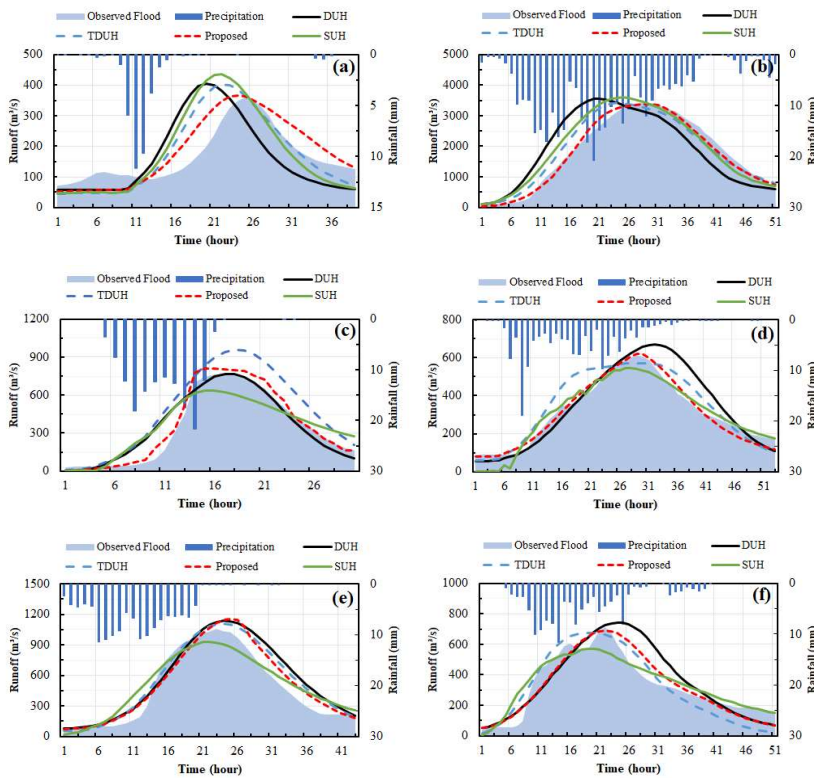
删除的内容: Proposed

20161021	0.89/1/0.89	1.08/1/0.83	1.05/1/0.89	1.10/2/0.91
20180606	0.84/4/0.78	1.20/3/0.68	1.13/4/0.72	0.97/2/0.84
20180830	0.97/2/0.83	1.05/2/0.75	1.06/1/0.82	1.05/2/0.81
20180916	0.80/3/0.86	1.05/2/0.62	0.95/3/0.81	0.97/1/0.85
Average	0.95/2.1/0.80	1.08/2.8/0.70	1.07/2.3/0.76	1.02/1.4/0.87

773 **Table 7.** Comparison of four routing methods for the Longhu River basin

Event number	$(Q_p^s / Q_p^o) / (t_p^s - t_p^o) / (E_{NS})$			
	SUH	DUH	TDUH	TDUH-MC_p
20030517	1.11/4/0.96	1.14/2/0.87	1.00/1/0.88	1.00/2/0.97
20060601	0.92/2/0.83	1.06/1/0.92	1.00/1/0.96	0.95/1/0.88
20060808	1.12/1/0.81	1.23/2/0.85	1.10/2/0.85	1.03/1/0.93
20120527	0.96/0/0.98	1.06/2/0.73	0.94/2/0.78	0.99/1/0.93
20130713	0.85/0/0.95	1.07/1/0.88	0.95/0/0.90	0.91/0/0.94
20161021	0.87/2/0.89	1.18/3/0.88	1.03/3/0.91	1.06/1/0.94

删除的内容: Proposed



778 **Figure 13.** Comparison of flow hydrographs obtained by the four methods. (a) Flow
779 event No.20130720. (b) Flow event No.20130817. (c) Flow event No.20150709. (d)
780 Flow event No.20160128. (e) Flow event No.20161021. (f) Flow event No.20180916.

781 For flow event No.20161021, the simulation result of the TDUH-MC method was
782 basically consistent with that of the TDUH method. This was because the antecedent
783 rainfall was close to saturation under this flow event. As a result, the TDUH-MC
784 method performed the same as the TDUH method when the watershed was saturated.

785 For flow event No.20180916, the simulation accuracy of the TDUH-MC method was
786 lower than that of the TDUH. The possible reason for the inaccurate flow simulation is
787 that the antecedent rainfall was relatively small. Because the runoff generation was not
788 dominated by the saturation-excess, and it was not appropriate to calculate runoff with
789 the XAJ model.

790 *5.4 Influence of time-varying soil moisture content on flow forecasts*

791 In order to evaluate the influence of time-varying soil moisture content on flow
792 forecasts, three typical flow forecast results of the TDUH-MC method were selected
793 for comparison in the Qin River basin. Specifically, compared with the forecasting
794 results using TDUH, results of flow event No.20130817 using the TDUH-MC method
795 were relatively similar, results of flow events No.20150709 and 20160128 had a better
796 performance, and results of flow event No.20180916 were poor. Their corresponding
797 temporal evolution of soil moisture content in unsaturated regions were obtained. The
798 box-and-whisker plots of soil moisture contents of all sub-basins for flow events

删除的内容: 11

删除的内容: 2

删除的内容: the

删除的内容: proposed

删除的内容: proposed

删除的内容: the

删除的内容: proposed

删除的内容: ing

删除的内容: proposed

删除的内容: the

删除的内容: the

删除的内容: proposed

删除的内容: the

删除的内容: the

删除的内容: the

删除的内容: the

815 No.20130817, 20150709, 20160128 and 20180916 are shown in Fig. 14. It can be seen
 816 from Fig. 14 that the soil moisture content of each sub-basin was initially low, then the
 817 soil moisture content of the sub-basin gradually increased. Meanwhile, it was obvious
 818 that θ_t was hard to reach the maximum value. For all flow events, 9 sub-basins
 819 eventually reached the saturation only under the condition of flow event No.20130817.
 820 The mean values of θ_t for flow events No.20150709, 20160128 and 20180916 ranged
 821 from 0.5 to 0.8, and the soil moisture content did not reach the maximum during the
 822 flow events. As shown from the observed flow in Fig. 13, the peak discharge of the
 823 flow event No.20130817 was larger than those of other flow events, reaching 3500 m³
 824 /s, which meant that the watershed more probably reached saturation during the flow
 825 period.

删除的内容: 12

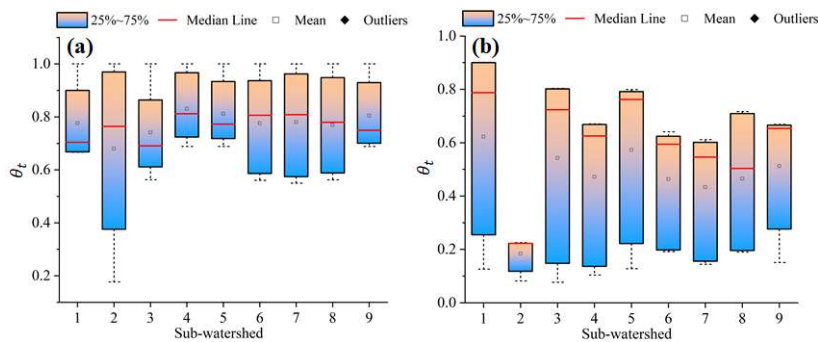
删除的内容: 3

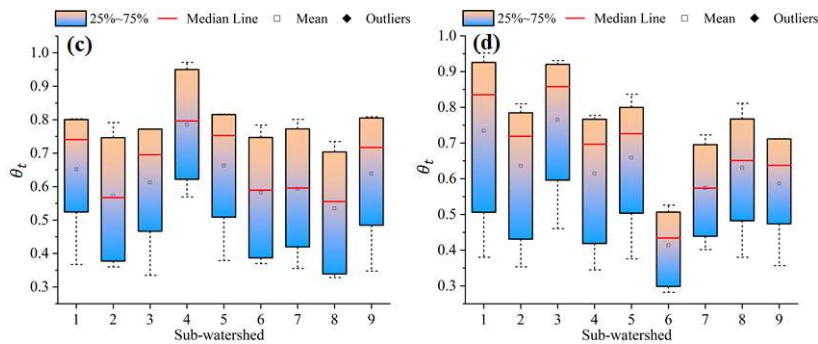
删除的内容: 12

删除的内容: 3

删除的内容: 10

826





832

833 **Figure 14.** Distributions of time-varying θ_t at different times in each sub-basin using
 834 the TDUH-MC method. (a) Flow event No.20130817. (b) Flow event No.20150709. (c)
 835 Flow event No.20160128. (d) Flow event No.20180916. θ_t represents the ratio of
 836 current soil moisture storage to the corresponding maximum soil moisture capacity in
 837 the unsaturated region.

838 As discussed in Section 5.3, results of flow event No.20130817 using the TDUH-
 839 MC routing method showed the same behavior as did TDUH. This was because the
 840 simulation performance of the TDUH-MC method considering time-varying soil
 841 moisture content was the same as that of TDUH when the soil moisture content was
 842 closer to 1. Additionally, the forecast results of flow events No.20150709, 20160128
 843 with the TDUH-MC routing method were obviously better than those of DUH and
 844 TDUH. The reason can be summarized as follows. The mean values of θ_t ranged from
 845 0.5 to 0.6 for the two flow events and the θ_t values were initially low as shown in Fig.
 846 14. Thus, the soil moisture content had a significant impact on the shape of the
 847 hydrograph. For flow event No.20180916, the sub-basins did not reach a global
 848 saturation, and the time-varying values of θ_t were generally high, which led to lower

删除的内容: 12
 删除的内容: 3
 删除的内容: proposed TDUH

删除的内容: the
 删除的内容: the
 删除的内容: proposed
 删除的内容: proposed

删除的内容: the
 删除的内容: proposed

删除的内容: 12
 删除的内容: 3
 删除的内容: the

861 flow velocity than in the TDUH method. The peak occurrence times of unit hydrographs
862 used for runoff routing calculations were general later, leading to a lag time between
863 maximum rainfall intensity and peak discharge for the forecast result of flow event
864 No.20180916.

删除的内容: ing
删除的内容: the

865 5.5 Comparison of velocity calculated by three DUH methods

866 The routing method considering both time-varying rainfall intensity and soil
867 moisture content was more accurate as discussed in Section 5.3. To evaluate the effect
868 of time-varying soil moisture content on flow velocity, we selected a grid cell in sub-
869 basin 3, in which slope and land type parameters were constant. Then, the flow velocity
870 was calculated under different storm conditions. The storm events No.20130817 and
871 20150709 were selected and compared, because storm event No.20130817 had a high
872 intensity and long duration, and storm event No. 20150709 had a short period of heavy
873 rainfall. Thus, soil moisture contents during the two storm events were significantly
874 different. Fig. 15 shows the time-varying velocity values of a grid cell for storm events
875 No.20130817 and 20150709. For the two storm events, the mean velocity of the DUH
876 method was the largest among the three methods, followed by the TDUH method. The
877 velocity calculated by the TDUH-MC method considering soil moisture content was
878 the smallest. The velocity of DUH method was constant in the two storms, and that of
879 the TDUH method varied with the change of excess rainfall. Meanwhile, the flow
880 velocity of the TDUH-MC method was not only dominated by rainfall intensity, but
881 was related to soil water content.

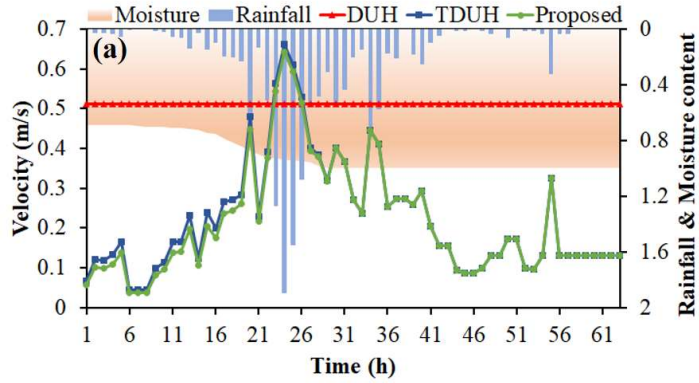
删除的内容: 13
删除的内容: 4

删除的内容: proposed

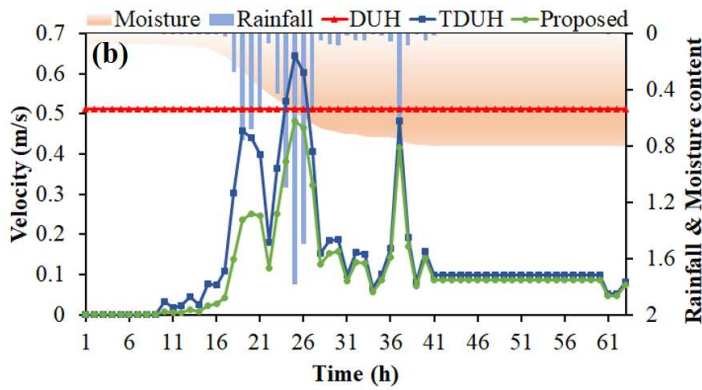
删除的内容: the

删除的内容: proposed

删除的内容: also



890



891

892 **Figure 15.** Time-varying velocity values of a grid cell in different storm events. (a)
 893 Time-varying velocity in storm event No.20130817. (b) Time-varying velocity in storm
 894 event No.20150709. The rainfall content is I_s , and the soil moisture content is θ_s .

895 For storm event No.20130817, the initial soil moisture content was large, and it
 896 reached the maximum rapidly. The flow velocity of the TDUH-MC method was slightly
 897 smaller than that of the TDUH method at the initial stage of storm events. When the
 898 whole basin reached saturation, the flow velocities of the two methods became equal.
 899 Therefore, the differences between hydrographs were small when using the TDUH

删除的内容: 13

删除的内容: 4

删除的内容: the

删除的内容: proposed

904 method and the TDUH-MC method for flow routing calculation, which led to similar
905 forecast results.

删除的内容: proposed

906 For storm event No.20150709, the initial soil moisture content was small, and the
907 entire basin could not reach the saturation after the rainstorm. Therefore, the grid
908 velocity in the early stage of the storm was greatly affected by the soil moisture content.

909 In the later stage of the rainstorm, θ_t of the watershed did not reach the maximum, but
910 was nearly close to 1. Thus, the impact of later soil moisture content on the flow velocity
911 was small. From the above analyses, it can be concluded that the shape and duration of
912 the unit hydrograph were mainly related to the soil moisture content at the initial stage
913 of a storm, and when the watershed was approximately saturated, the grid flow velocity
914 was mainly dominated by the excess rainfall.

删除的内容: and

915 5.6 Sensitivity analysis for the TDUH-MC method

删除的内容: proposed TDUH

916 A sensitivity analysis for the proposed formula was made in the Longhu River
917 basin. The improved method is only with two additional parameters, compared with the
918 current model. The objective of this study was to explore the influence soil moisture
919 content factor on the performance of the DUH model. Parameter γ in Eq. (3)
920 significantly affected the significant degree of influence over how large that soil
921 moisture content will be. Thus, sensitivity analysis for parameter γ was necessary. A
922 specific grid cell in the Longhu River basin was taken as an example, where the slope
923 of the grid cell was set to 0.22 m/m. The coefficient of flow velocity k and the ratio of
924 rainfall intensity to the reference rainfall intensity I_s were assumed to be 1.5 m/s and 1,

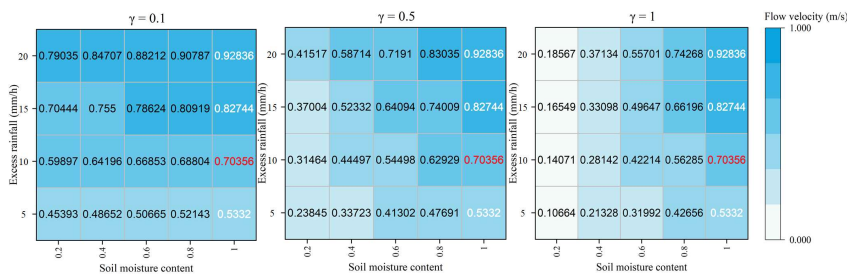
删除的内容: conducted

删除的内容: is

删除的内容: The p

删除的内容: mainly

932 respectively. When parameter γ was 0.1, 0.5 and 1, respectively, the hillslope flow
 933 velocity values corresponding to different rainfall and soil moisture contents using the
 934 proposed formula are given in Fig. 16.



删除的内容: 14
 删除的内容: 5

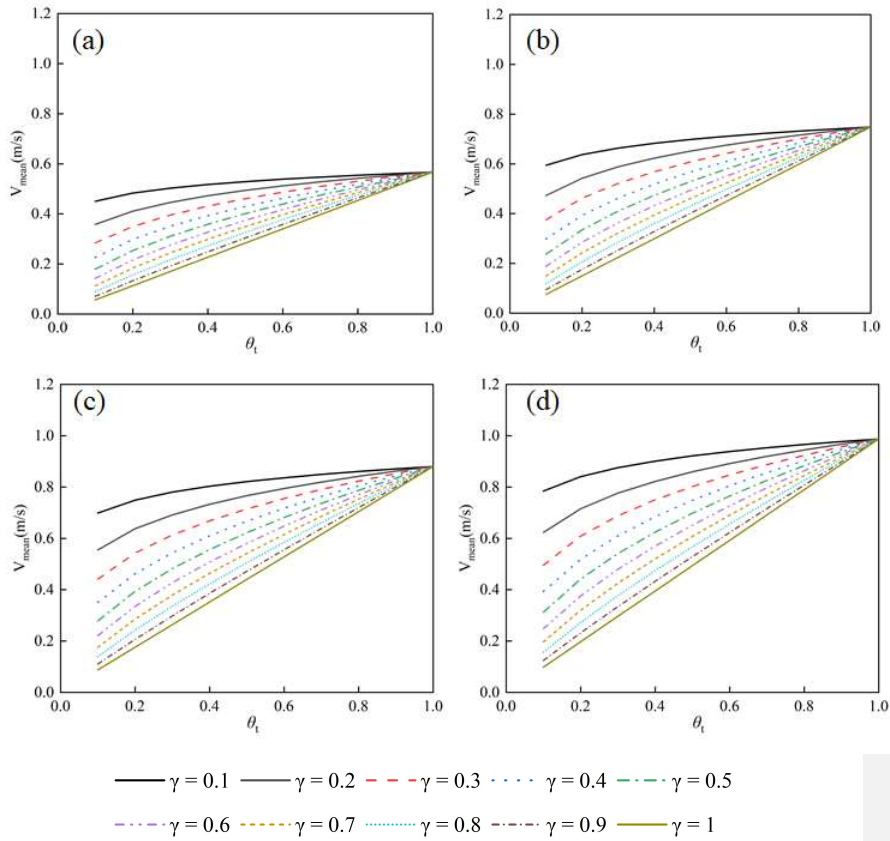
935
 936 **Figure 16.** Time-varying flow velocity values corresponding to different parameters

937 It can be seen from Fig. 16 that when θ_i was equal to 1, the proposed Eq. (3)
 938 turned to Eq. (2). The flow velocity values in the last column were the same and only
 939 changed with rainfall intensities. When I_i was equal to the reference rainfall I_c , Eq. (2)
 940 turned to Eq. (1), and the flow velocity was 0.704 m/s. After introducing a soil moisture
 941 content factor into the flow velocity formula, the flow velocity values ranged from
 942 0.107 m/s to 0.928 m/s when γ was equal to 1. The flow velocity values were
 943 significantly different corresponding to different values of parameter γ . Thus, the
 944 parameter γ significantly affected the performance of the new routing method.

删除的内容: 14
 删除的内容: 5
 删除的内容: 14
 删除的内容: 5

945 Moreover, the mean flow velocity of the Longhu River basin was calculated under
 946 different rainfall intensities (e.g. $\frac{I_i}{I_c} = 0.5, 1, 1.5, 2$, respectively). Fig. 17 plots the
 947 theoretical curve of mean velocity and soil moisture content.

删除的内容: 15
 删除的内容: 6



956

957

958 **Figure 17.** The theoretical curve of mean velocity and soil moisture content for the
 959 Longhu River basin. (a) $\frac{I_t}{I_c} = 0.5$. (b) $\frac{I_t}{I_c} = 1$. (c) $\frac{I_t}{I_c} = 1.5$. (d) $\frac{I_t}{I_c} = 2$.

960 Fig. 17 reveals that the mean flow velocity ranged from 0.6 to 1 under different
 961 rainfall intensities without considering the influence of soil moisture content. After
 962 introducing this new factor into the current flow velocity formula, the mean flow
 963 velocity was significantly influenced by exponent γ . In addition, when the soil
 964 moisture content exceeded 0.7, the variation range of mean flow velocity decreased
 965 sharply. Results showed that the influence of parameter γ on the flow velocity

删除的内容: 15

删除的内容: 6

删除的内容: 15

删除的内容: 6

删除的内容: shows

删除的内容: the

972 decreased gradually with the increase of soil moisture content.

973 **5. Conclusions**

974 An improved distributed unit hydrograph method considering time-varying soil
975 moisture content was proposed for flow routing. The ~~TDUH-MC~~ method
976 comprehensively considered the changes of time-varying soil moisture content and
977 rainfall intensity. The response of the underlying surface to the soil moisture content
978 was considered as an important factor. The Qin River basin and Longhu River basin
979 were selected as two case studies. The SUH, DUH, TDUH and ~~TDUH-MC~~ routing
980 methods were used for flow forecasting, and simulated results were compared. The
981 sensitivity analysis was conducted for parameter γ . The main conclusions can be
982 summarized as follows.

983 (1) The ~~TDUH-MC~~ runoff routing method, considering both time-varying rainfall
984 intensity and soil moisture content, was proposed, and the influence of the
985 inhomogeneity of runoff generation on the routing process was considered. It was found
986 that the soil moisture content was a significant factor affecting the accuracy of flow
987 forecast, especially in the catchment dominated by saturation-excess runoff, and the
988 flow velocity increased gradually with more surface runoff after considering the soil
989 moisture content in unsaturated regions.

990 (2) The time-varying characteristics of the DUH can be further considered by
991 introducing both rainfall intensity and soil moisture content into the flow velocity

删除的内容: proposed

删除的内容: proposed

删除的内容: proposed

删除的内容: s

996 formula, which can effectively improve the accuracy of flow forecasts. Simulation
997 hydrographs and criteria of the two case studies showed that the accuracy of the TDUH-
998 MC method was the highest, followed by the SUH and TDUH methods, and finally the
999 DUH method.

删除的内容: proposed

1000 (3) The shape and duration of the improved TDUH considering soil moisture were
1001 mainly affected by rainfall intensity. Meanwhile, soil moisture content at the initial
1002 stage of a storm also played a significant role in the characteristics of the improved
1003 TDUH. When the watershed was approximately saturated, the grid flow velocity was
1004 mainly dominated by excess rainfall.

删除的内容: is

1005 (4) Results of sensitivity analysis showed that the accuracy of the TDUH-MC
1006 method was mainly affected by soil moisture content. The influence of parameter γ
1007 on the flow velocity decreased gradually with the increase of soil moisture content.

删除的内容: proposed

1008 **Data availability**

1009 Due to the strict security requirements from the departments, some or all data, models,
1010 or code generated or used in the study are proprietary or confidential in nature and may
1011 only be provided with restrictions (e.g. anonymized data).

1012 **Author contributions**

1013 Lu Chen conceived the original idea, and Bin Yi designed the methodology. Ping Jiang
1014 collected the data. Bin Yi developed the code and performed the study. Bin Yi, Lu Chen,
1015 Hansong Zhang and Vijay P. Singh contributed to the interpretation of the results. Bin

1019 Yi wrote the paper, and Lu Chen, Vijay P. Singh revised the paper.

1020 **Competing interests**

1021 The authors declare that they have no conflict of interest.

1022 **Acknowledgments**

1023 This research has been supported by the National Outstanding Youth Science Fund
1024 Project of National Natural Science Foundation of China (No. 51922047), and the
1025 General Program of National Natural Science Foundation of China (No. 51879109).

1026 **References**

- 1027 Anderson, AE, Weiler, et al., Hudson Subsurface flow velocities in a hillslope with
1028 lateral preferential flow. *Water Resources Research*, 45, pp. W11407,
1029 <https://doi.org/10.1029/2008WR007121>, 2009.
- 1030 [Akram, F., Rasul, M. G., Khan, M. M. K., et al. Comparison of different hydrograph
1031 routing techniques in XPSTORM modelling software: A case study. *International
1032 Journal of Environmental and Ecological Engineering*, 8\(3\): 213-223,
1033 <https://doi.org/10.5281/zenodo.1093034>, 2014.](#)
- 1034 [Bhunya, P. K., Ghosh, N. C., Mishra, S. K., Ojha, C. S. and Berndtsson, R.: Hybrid
1035 Model for Derivation of Synthetic Unit Hydrograph. *Journal of Hydrologic
1036 Engineering*, 10\(6\):458-467, \[https://doi.org/10.1061/\\(ASCE\\)1084-
1038 0699\\(2005\\)10:6\\(458\\)\]\(https://doi.org/10.1061/\(ASCE\)1084-
1037 0699\(2005\)10:6\(458\)\), 2005.](#)
- 1038 Beskow, S., Mello, C. R., Norton, L. D. and da Silva, A. M.: Performance of a
1039 distributed semi-conceptual hydrological model under tropical watershed
1040 conditions. *Catena*, 86(3):160-171, <https://doi.org/10.1016/j.catena.2011.03.010>,
1041 2011.
- 1042 Bhattacharya, A. K., McEnroe, B. M., Zhao, H., Kumar, D., and Shinde, C.: Modclark
1043 model: improvement and application. *Journal of Engineering*, 2(7):100-118,
1044 <https://doi.org/10.9790/3021-0271100118>, 2012.
- 1045 Brenden, J., Stefan H. S., Luc, F., Jeroen, C. J. H. Aerts, Reinhard, M., Wouter Botzen,
1046 W. J., Laurens M. B., Georg, P., Rodrigo, R. and Philip, J. W.: Increasing stress on
1047 disaster-risk finance due to large floods. *Nature Climate Change*, 4(4):264-268,
1048 <https://doi.org/10.1038/nclimate2124>, 2014.
- 1049 Bhuyan, M. K., Kumar, S., Jena, J. and Bhunya, P. K.: Flood Hydrograph with Synthetic

删除的内容: Alfieri, L., Burek, P., Feyen, L. and Forzieri, G.: Global warming increases the frequency of river floods in Europe. *Hydrology and Earth System Sciences*. 19:2247-2260, <https://doi.org/10.5194/hess-19-2247-2015>, 2015. .

1054 Unit Hydrograph Routing. *Water Resources Management*, 29(15):5765-5782,
1055 <https://doi.org/10.1007/s11269-015-1145-1>, 2015.

1056 Bunster, T., Gironás, J., Niemann, J. D.: On the Influence of Upstream Flow
1057 Contributions on the Basin Response Function for Hydrograph Prediction. *Water*
1058 *Resources Research*, 55 (6), 4915-4935, <https://doi.org/10.1029/2018WR024510>,
1059 2019.

1060 Brunner M. I., Swain D. L., Wood R. R., Willkofer F., Done J. M., Gilleland E., Ludwig
1061 R. An extremeness threshold determines the regional response of floods to changes
1062 in rainfall extremes. *Communications Earth & Environment*, 2(1),
1063 <https://doi.org/10.1038/s43247-021-00248-x>, 2021.

1064 Clark, C. O.: Storage and the unit hydrograph. *Transactions*, 69(9):1333-1360,
1065 <https://doi.org/10.1061/TACEAT.0005800>, 1945.

1066 [Chow, V. T.: *Open Channel Hydraulics*, McGraw-Hill, New York, USA, 1959.](#)

1067 Chow, V. T.: Handbook of applied hydrology. *Hydrological Sciences Journal*, 10(1),
1068 1964.

1069 Chow, V. T., Maidment, D. R., and Mays, L. W. *Applied hydrology*, McGraw-Hill, New
1070 York, 1988.

1071 [Chu, H. J., Chang, L. C.: *Applying Particle Swarm Optimization to Parameter*](#)
1072 [Estimation of the Nonlinear Muskingum Model. *Journal of Hydrologic*](#)
1073 [Engineering](#), 14(9):1024-1027, [https://doi.org/10.1061/\(ASCE\)HE.1943-5584.0000070](https://doi.org/10.1061/(ASCE)HE.1943-5584.0000070), 2009.

1075 Chinh, L., Iseri, H., Hiramatsu, K., Harada, M. and Mori, M.: Simulation of rainfall
1076 runoff and pollutant load for Chikugo River basin in Japan using a GIS-based
1077 distributed parameter model. *Paddy and Water Environment*, 11(1-4):97-112,
1078 <https://doi.org/10.1007/s10333-011-0296-9>, 2013.

1079 Chen, L., Zhang, Y. C., Zhou, J. Z., Guo, S. L. and Zhang, J. H.: Real-time error
1080 correction method combined with combination flood forecasting technique for
1081 improving the accuracy of flood forecasting. *Journal of hydrology*, 2015, 521: 157-
1082 169, <https://doi.org/10.1016/j.jhydrol.2014.11.053>, 2015.

1083 Chen, L., Gan, X. X., Yi, B., Qin, Y. H. P. and Lu, L. Q. Domestic water demand
1084 prediction based on system dynamics combined with social-hydrology methods.
1085 *Hydrology Research*, 53(8), 1107-1128, <https://doi.org/10.2166/nh.2022.051>, 2022.

1086 Chen, L., Ge, L. S., Wang, D. W., Zhong, W. J., Zhan, T. and Deng, A.: Multi-objective
1087 water-sediment optimal operation of cascade reservoirs in the Yellow River Basin.
1088 *Journal of hydrology*, 609:127744, <https://doi.org/10.1016/j.jhydrol.2022.127744>,
1089 2022a.

1090 Chen, L., Hou, B. Q., Zhan, T., Ge, L. S., Qin, Y. H. P. and Zhong, W. J.: Water-
1091 sediment-energy joint operation model of large-scale reservoir group for sediment-
1092 laden rivers. *Journal of Cleaner Production*, 370, 133271,
1093 <https://doi.org/10.1016/j.jclepro.2022.133271>, 2022b.

1094 Dooge, J.: A General Theory of the Unit Hydrograph. *Journal of Geophysical Research*
1095 *Atmospheres*, 64(2):241-256, <https://doi.org/10.1029/JZ064i002p00241>, 1959.

域代码已更改

带格式的: 无下划线, 字体颜色: 自动设置

1096 Duan, Q. Y., Sorooshian, S., Gupta, V.: Effective and efficient global optimization for
1097 conceptual rainfall-runoff models. *Water Resources Research*. 28(4):1015-1031,
1098 <https://doi.org/10.1029/91WR02985>, 1992.

1099 Du, J., Xie, H., Hu, Y., Xu, Y. P. and Xu, C. Y.: Development and testing of a new storm
1100 runoff routing approach based on time variant spatially distributed travel time
1101 method. *Journal of Hydrology*, 369(1-2):44-54,
1102 <https://doi.org/10.1016/j.jhydrol.2009.02.033>, 2009.

1103 Gupta, V. K., Waymire, E., Wang, C. T.: A representation of an instantaneous unit
1104 hydrograph from geomorphology. *Water Resources Research*, 16(5): 855-862,
1105 <https://doi.org/10.1029/WR016i005p00855>, 1980.

1106 Gupta, H. V., Kling, H., Yilmaz, K. K. & Martinez, G. F. Decomposition of the mean
1107 squared error and NSE performance criteria: Implications for improving
1108 hydrological modelling. *Journal of Hydrology*. 377, 80-91,
1109 <https://doi.org/10.1016/j.jhydrol.2009.08.003>, 2009.

1110 Gironás, J., Niemann, J. D., Roesner, L. A., Rodriguez, F. and Andrieu, H.: A morpho-
1111 climatic instantaneous unit hydrograph model for urban catchments based on the
1112 kinematic wave approximation. *Journal of Hydrology*, 377(3-4),
1113 <https://doi.org/10.1016/j.jhydrol.2009.08.030> 317–334, 2009.

1114 Gibbs, M. S., Dandy, G. C., Maier, H. R.: Evaluation of parameter setting for two GIS
1115 based unit hydrograph models. *Journal of Hydrology*, 393(3-4), 197–205,
1116 <https://doi.org/10.1016/j.jhydrol.2010.08.014>, 2010.

1117 Grimaldi, S., Petroselli, A., Alonso, G., Nardi, F. Flow time estimation with spatially
1118 variable hillslope velocity in ungauged basins. *Advances in Water Resources*, 33
1119 (10), 1216-1223, <https://doi.org/10.1016/j.advwatres.2010.06.003>, 2010.

1120 Grimaldi, S., Petroselli, A., Nardi, F. A parsimonious geomorphological unit
1121 hydrograph for rainfall-runoff modelling in small ungauged basins. *Hydrological
1122 Sciences Journal*, 57 (1), 73-83, <https://doi.org/10.1080/02626667.2011.636045>,
1123 2012.

1124 Gad, M. A.: Flow Velocity and Travel Time Determination on Grid Basis Using
1125 Spatially Varied Hydraulic Radius. *Journal of Environmental Informatics*,
1126 <https://doi.org/10.3808/jei.201400259>, 23(2):36-46, 2014.

1127 Haan, C.T., Barfield, B.J., Hays J.C.: *Design hydrology and sedimentology for small
1128 catchments* Academic Press, New York, 1994.

1129 Hutchinson, D. G., and R. D. Moore, Throughflow variability on a forested hillslope
1130 underlain by compacted glacial till, *Hydrol. Processes*,14(10), 1751-1766,
1131 [https://doi.org/10.1002/1099-1085\(200007\)14:10<1751::AID-HYP68>3.0.CO;2-
1132 U](https://doi.org/10.1002/1099-1085(200007)14:10<1751::AID-HYP68>3.0.CO;2-U), 2000.

1133 James, W., Johanson, R. C. A Note on an Inherent Difficulty with the Unit Hydrograph
1134 Method. *Journal of Water Management Modeling*,
1135 <https://doi.org/10.14796/JWMM.R204-01>, 1999.

1136 Katz, D. M., Watts, F. J., Burroughs, E. R. Effects of Surface Roughness and Rainfall
1137 Impact on Overland Flow. *Journal of Hydraulic Engineering*, 121(7):546-553,

1138 [https://doi.org/10.1061/\(ASCE\)0733-9429\(1995\)121:7\(546\)](https://doi.org/10.1061/(ASCE)0733-9429(1995)121:7(546)), 1995.

1139 Kilgore, J. L. Development and evaluation of a GIS - based spatially distributed unit
 1140 hydrograph model, (Master's thesis). Blacksburg, VA: Virginia Polytechnic
 1141 Institute and State University. <http://hdl.handle.net/10919/35777>, 1997.

1142 Kumar, R., Chatterjee, C., Singh, R. D., Lohani, A. K. and Kumar, S.: Runoff estimation
 1143 for an ungauged catchment using geomorphological instantaneous unit
 1144 hydrograph (GIUH) models. *Hydrological Processes*, 21(14):1829-1840,
 1145 <https://doi.org/10.1002/hyp.6318>, 2007.

1146 Khaleghi, S., Monajemi, P., Nia, M. P.: Introducing a new conceptual instantaneous unit
 1147 hydrograph model based on a hydraulic approach. *Hydrological Sciences Journal*,
 1148 63:13-14, <https://doi.org/10.1080/02626667.2018.1550294>, 2018.

1149 Kong, F. Z., Guo, L.: A method of deriving time-variant distributed unit hydrograph.
 1150 *Advances in Water Science*, 30(04):477-484,
 1151 <https://doi.org/10.14042/j.cnki.32.1309.2019.04.003>. 2019. (in chinese)

1152 Linsley, R. K., Kohler, M. A., Paulhus, J. L. *Applied hydrology*. The McGraw-Hill
 1153 Book company, Inc., New York, 1949.

1154 Lee, K. T., Chen, N. C., Chung, Y. R.: Derivation of variable IUH corresponding to
 1155 time-varying rainfall intensity during storms. *International Association of*
 1156 *Scientific Hydrology Bulletin*, 53(2):323-337,
 1157 <https://doi.org/10.1623/hysj.53.2.323>, 2008.

1158 Mockus, V.: Use of storm and watershed characteristics in synthetic hydrograph
 1159 analysis and application. AGU, Pacific Southwest Region Mtg., Sacramento, Calif,
 1160 1957.

1161 Minshall, N. E.: Predicting storm runoff on small experimental watersheds. *J. Hydraul.*
 1162 *Engng ASCE*, 86(HY8), 17-38, <https://doi.org/10.1061/JYCEAJ.0000509>, 1960.

1163 Moore, R. J.: The probability-distributed principle and runoff production at point and
 1164 basin scales, *Hydrological Sciences Journal*, 30, 273-297,
 1165 <https://doi.org/10.1080/02626668509490989>, 1985.

1166 Maidment, D. R.: Developing a spatially distributed unit hydrograph by using GIS.
 1167 IAHS publication, 181-181, 1993.

1168 Maidment, D. R., Olivera, F., Calver, A., Eatherall, A. and Fraczek, W.: Unit
 1169 hydrograph derived from a spatially distributed velocity field. *Hydrological*
 1170 *Processes*, 10: 831-844, [https://doi.org/10.1002/\(SICI\)1099-1085\(199606\)10:6<831::AID-HYP374>3.0.CO;2-N](https://doi.org/10.1002/(SICI)1099-1085(199606)10:6<831::AID-HYP374>3.0.CO;2-N), 1996.

1172 Muzik, I.: A GIS-derived distributed unit hydrograph. *Hydrological Processes*,
 1173 10(10):1401-1409, [https://doi.org/10.1002/\(SICI\)1099-1085\(199610\)10:10<1401::AID-HYP469>3.0.CO;2-3](https://doi.org/10.1002/(SICI)1099-1085(199610)10:10<1401::AID-HYP469>3.0.CO;2-3), 1996.

1175 Martinez, V., Garcia, A. I., Ayuga, F.: Distributed routing techniques developed on GIS
 1176 for generating synthetic unit hydrographs. *Transactions of the ASAE*, 45(6):1825-
 1177 1834, <https://doi.org/10.13031/2013.11433>, 2002.

1178 Melesse, A. M., Graham, W. D.: Storm runoff prediction based on a spatially distributed
 1179 travel time method utilizing remote sensing and GIS, *Journal of the American*

1180 Water Resources Association, 40 (4), 863-879, <https://doi.org/10.1111/j.1752->
1181 1688.2004.tb01051.x, 2004.

1182 [Moghaddam, A., Behmanesh, J., Farsijani, A.: Parameters estimation for the new four-](#)
1183 [parameter nonlinear Muskingum model using the particle swarm optimization,](#)
1184 [Water Resour. Manage., 30 \(7\), 2143-2160, https://doi.org/10.1007/s11269-016-](#)
1185 [1278-x, 2016.](#)

1186 [Mizukami, N., Rakovec, O., Newman, A. J., Clark, M. P., Wood, A. W., Gupta, H. V.,](#)
1187 [and Kumar, R.: On the choice of calibration metrics for “high-flow” estimation](#)
1188 [using hydrologic models, Hydrology and Earth System Sciences, 23, 2601-2614,](#)
1189 [https://doi.org/10.5194/hess-23-2601-2019, 2019.](#)

1190 Nash, J. E.: The form of the instantaneous unit hydrograph. International Association
1191 of Science and Hydrology, 45(3):114-121, 1957.

1192 Nash, J. E. & Sutcliffe, I. V. River flow forecasting through conceptual models part I -
1193 a discussion of principles. Journal of Hydrology, 10, 282-290,
1194 [https://doi.org/10.1016/0022-1694\(70\)90255-6](https://doi.org/10.1016/0022-1694(70)90255-6), 1970.

1195 NRCS (natural Resources Conservation Service), Ponds Planning, design, construction.
1196 Washington, DC: US Natural Resources Conservation Service, Agriculture
1197 Handbook no.590, 1997.

1198 Noto, L. V., Loggia, G. L.: Derivation of a distributed unit hydrograph integrating GIS
1199 and remote sensing. Journal of Hydrologic Engineering, 12 (6):639-650,
1200 [https://doi.org/10.1061/\(ASCE\)1084-0699\(2007\)12:6\(639\)](https://doi.org/10.1061/(ASCE)1084-0699(2007)12:6(639)), 2007.

1201 [Nourani, V., Singh, V. P., Delafrouz, H. Three geomorphological rainfall-runoff models](#)
1202 [based on the linear reservoir concept. Catena, 76\(3\): 206-214,](#)
1203 [https://doi.org/10.1016/j.catena.2008.11.008, 2009.](#)

1204 Nigussie T. A., Yeğen E. B., Melesse A. M.: Performance Evaluation of Synthetic Unit
1205 Hydrograph Methods in Mediterranean Climate. A Case Study at Guvenc Micro-
1206 watershed, Turkey. In: Melesse A., Abteu W. (eds) Landscape Dynamics, Soils
1207 and Hydrological Processes in Varied Climates. Springer Geography. Springer,
1208 Cham. https://doi.org/10.1007/978-3-319-18787-7_15, 2016.

1209 Peters, D. L., et al. Runoff production in a forested, shallow soil, Canadian Shield Basin,
1210 Water Resources Research, 31(5), 1291-1304, doi:10.1029/94WR03286, 1995.

1211 [Ponce, V. M., Lohani, A. K., Scheyhing, C.: Analytical verification of Muskingum-](#)
1212 [Cunge routing. Journal of Hydrology, 174\(3-4\): 235-241,](#)
1213 [https://doi.org/10.1016/0022-1694\(95\)02765-3, 1996.](#)

1214 [Petroselli, A., Grimaldi, S. Design hydrograph estimation in small and fully ungauged](#)
1215 [basins: a preliminary assessment of the EBA4SUB framework. Journal of Flood](#)
1216 [Risk Management, 11: S197-S210, https://doi.org/10.1111/jfr3.12193, 2018.](#)

1217 Paul, P. K., Kumari, N., Panigrahi, N., Mishra, A. and Singh, R.: Implementation of
1218 cell-to-cell routing scheme in a large scale conceptual hydrological model
1219 Environmental Modelling & Software, 101(C):23-33,
1220 <https://doi.org/10.1016/j.envsoft.2017.12.003>, 2018.

1221 Rodríguez-Iturbe, I., Valdes, J. B.: The geomorphologic structure of hydrologic

删除的内容: Munich, R. E.: Natural catastrophe losses at their highest for four years, 2017. .

1224 response. *Water Resources Research*, 15(6): 1409-1420,
1225 <https://doi.org/10.1029/WR015i006p01409>, 1979.

1226 Rodríguez-Iturbe, I., González-Sanabria, M., Bras R. L.: A geomorphoclimatic theory
1227 of the instantaneous unit hydrograph. *Water Resources Research*, 18(4):877-886,
1228 <https://doi.org/10.1029/WR018i004p00877>, 1982.

1229 Rigon, R., Bancheri, M., Formetta, G. and Lavenne, A.: The geomorphological unit
1230 hydrograph from a historical-critical perspective[J]. *Earth Surface Processes &
1231 Landforms*, 41(1):27-37, <https://doi.org/10.1002/esp.3855>, 2016.

1232 Sherman, L. K.: Streamflow from rainfall by the unit-graph method. *Engineering News
1233 Record*, 108:501-505, 1932.

1234 Snyder, F. F.: Synthetic unit-graphs. *Transactions American Geophysical Union*, 19,
1235 447-454, <https://doi.org/10.1029/TR019i001p00447>, 1938.

1236 Steenhuis, T. S., et al. Preferential flow influences on drainage of shallow sloping soils,
1237 *Agric. Water Manage.*, 14(1-4), 137-151, [https://doi.org/10.1016/0378-
1238 3774\(88\)90069-8](https://doi.org/10.1016/0378-3774(88)90069-8), 1988.

1239 Saghafian, B., Julien, P. Y.: Time to equilibrium for spatially variable watersheds.
1240 *Journal of Hydrology*, 172 (1-4):231-245, [https://doi.org/10.1016/0022-
1241 1694\(95\)02692-I](https://doi.org/10.1016/0022-1694(95)02692-I), 1995.

1242 Sidle, R. C., et al. Stormflow generation in steep forested head-waters: A linked
1243 hydrogeomorphic paradigm, *Hydrological Processes*, 14(3), 369-385,
1244 [https://doi.org/10.1002/\(SICI\)1099-1085\(20000228\)14
1245 :3<369::AID-HYP943>3.0.CO;2-P](https://doi.org/10.1002/(SICI)1099-1085(20000228)14:3<369::AID-HYP943>3.0.CO;2-P), 2000.

1246 Sidle, R. C., et al. A conceptual model of preferential flow systems in forested hillslopes:
1247 Evidence of self-organization, *Hydrological Processes*, 15(10), 1675-1692,
1248 <https://doi.org/10.1002/hyp.233>, 2001.

1249 SCS. Design of hydrograph. Washington, DC: US Department of Agriculture, Soil
1250 Conservation Service. 2002.

1251 Sarangi, A., Madramootoo, C. A., Enright, P. and Prasher, S. O.: Evaluation of three
1252 unit hydrograph models to predict the surface runoff from a Canadian watershed.
1253 *Water Resources Management*, 21(7):1127-1143, [https://doi.org/10.1007/s11269-
1254 006-9072-9](https://doi.org/10.1007/s11269-006-9072-9), 2007.

1255 [Singh V.P.: Hydrologic Systems, Rainfall-Runoff Modeling, vol. I, Prentice-Hall,
1256 Englewood Cliffs, 1988.](#)

1257 Singh, P. K., Bhunya, P. K., Mishra, S. K. and Chaube, U. C.: An extended hybrid model
1258 for synthetic unit hydrograph derivation. *Journal of Hydrology*, 336(3-4):347-360,
1259 <https://doi.org/10.1016/j.jhydrol.2007.01.006>, 2007.

1260 Singh, P. K., Mishra, S. K. and Jain, M. K.: A review of the synthetic unit hydrograph:
1261 from the empirical UH to advanced geomorphological methods. *International
1262 Association of Scientific Hydrology Bulletin*, 59(2):239-261,
1263 <https://doi.org/10.1080/02626667.2013.870664>, 2014.

1264 Singh, S. K.: Simple Parametric Instantaneous Unit Hydrograph. *Journal of Irrigation
1265 & Drainage Engineering*, 141(5):04014066.1-04014066.10,

1266 [https://doi.org/10.1061/\(ASCE\)IR.1943-4774.0000830](https://doi.org/10.1061/(ASCE)IR.1943-4774.0000830), 2015.

1267 Singh, V.P.: Hydrologic Systems: Vol. 1. Rainfall-Runoff Modeling. Prentice Hall,
1268 Englewood Cliffs, New Jersey.

1269 Tsuboyama, Y., et al. Flow and solute transport through the soilmatrix and macropores
1270 of a hillslope segment, Water Resources Research, 30(4),879-890,
1271 <https://doi.org/10.1029/93WR03245>, 1994.

1272 Tani, M. Runoff generation processes estimated from hydrological observations on a
1273 steep forested hillslope with a thin soil layer, Journal of Hydrology, 200(1-4), 84-
1274 109, [https://doi.org/10.1016/S0022-1694\(97\)00018-8](https://doi.org/10.1016/S0022-1694(97)00018-8), 1997.

1275 Vrugt, J. A., Gupta, H. V., Dekker, S. C., Sorooshian, S., Wagener, T. and Bouten, W.:
1276 Application of stochastic parameter optimization to the Sacramento Soil Moisture
1277 Accounting model. Journal of Hydrology, 325(1-4), 288-307,
1278 <https://doi.org/10.1016/j.jhydrol.2005.10.041>, 2006.

1279 [Wilson, B. N., Ruffini, J. R.: Comparison of physically based Muskingum methods.](#)
1280 [Transactions of ASAE, 31\(1\): 91-97, https://doi.org/10.13031/2013.30671, 1988.](#)

1281 Wong, T. S. W. Time of concentration formulae for planes with upstream inflow.
1282 Hydrological Sciences Journal, 40(5), 663-666.
1283 <https://doi.org/10.1080/02626669509491451>, 1995.

1284 [Yue, S., Hashino, M. Unit hydrographs to model quick and slow runoff components of](#)
1285 [streamflow. Journal of Hydrology, 227\(1-4\): 195-206,](#)
1286 [https://doi.org/10.1016/S0022-1694\(99\)00185-7, 2000.](#)

1287 Zhao, R. J., Zuang, Y., Fang, L.: The xinanjiang model. IAHS AISH Publ. 129, 351-
1288 356, 1980.

1289 Zhao, R. J.: Xinanjiang model applied in China. J. Hydrol. 135(1-4), 371-381,
1290 [https://doi.org/10.1016/0022-1694\(92\)90096-E](https://doi.org/10.1016/0022-1694(92)90096-E), 1992.

1291 Zhou, Q., Chen, L., Singh, V. P., Zhou, J. Z., Chen, X. H. and Xiong, L. H.: Rainfall-
1292 runoff simulation in Karst dominated areas based on a coupled conceptual
1293 hydrological model. Journal of Hydrology, 573: 524-533,
1294 <https://doi.org/10.1016/j.jhydrol.2019.03.099>, 2019.

带格式的：两端对齐，缩进：左侧：0 厘米，悬挂缩进：2 字符，首行缩进：-2 字符，行距：单倍行距